Mathematical Analysis of an Age- and Socioeconomic-Stratified COVID-19 Transmission Model

Gbeminiyi J. Oyedele [1,4,*‡], Oluwarimi J. Idowu [3‡], Michael J. Tildesley [1,2‡],

1 University of Warwick, Institute for global and Pandemic Planning, Coventry, CV4 7AL, UK
2 University of Warwick, School of Life Sciences and Mathematics Institute, Coventry, CV4 7AL, UK
3 University of Benin, Department of Mathematics, Benin, P.M.B. 1154, Nigeria
4 University of Warwick, Warwick Medical School, Coventry, CV4 7AL, UK

‡These authors also contributed equally to this work.
* gbeminiyi.oyedele@warwick.ac.uk

Abstract

The COVID-19 pandemic has sparked significant interest in developing mathematical models that capture more of the complexities of the dynamics of disease transmission and control. In this study, we presented a deterministic compartmental model for the transmission of COVID-19. The model has eight compartments: susceptible, exposed, asymptomatic, unreported symptomatic, reported symptomatic, hospitalised, recovered, and dead. Individuals in each compartment are discretised into age and deprivation deciles to study the combined effect of both factors on disease dynamics. We analyse the model and present the results for both the disease-free and endemic equilibrium states. We evaluate the basic reproduction number using a next-generation matrix approach. We also prove the local and global stability of the disease-free and endemic equilibria. Sensitivity indices are calculated both analytically and numerically to identify the parameters that have the greatest influence on R_0. Our results suggest that transmission, recovery, treatment, and testing rates need to be closely monitored to reduce the disease burden. Specifically, prompt testing, treatment, and recovery are critical for reducing R_0.

1 Introduction

COVID-19 has resulted in an unprecedented global health crisis, significant changes in the world's social structure, and widespread economic consequences. The transmission of SARS-CoV-2 occurs mainly via respiratory droplets and direct contact with infected surfaces [1]. The disease presents with diverse symptoms, ranging from a mild cough, fever, and fatigue to severe pneumonia [1]. Understanding the dynamics of COVID-19 transmission can provide valuable information regarding the most effective intervention strategies to mitigate the ongoing impact of the virus. The aim of this study is to develop and analyse a novel mathematical model that integrates an age and deprivation-decile contact mixing structure and time-dependent testing capacity to better understand disparities in infectious disease transmission and control. By incorporating these factors into the contact structure of a compartmental model, we can evaluate their impact on disease spread, analytically study stability conditions, and

identify key parameters influencing transmission dynamics. The objective is to provide actionable insights for targeted public health interventions, especially in mitigating the disparities in infectious burdens across deprivation deciles.

The transmission and control of COVID-19 have been extensively studied using mathematical models since the SARS-CoV-2 virus emerged in late 2019 [2–4]. Epidemiologists have worked closely with policymakers using various modelling techniques to provide guidance on disease outbreaks. The resulting models have been helpful in addressing several critical questions, including the projected final size of a given outbreak, the estimated number of individuals who will be infected, the timing of the peak of infection, and the optimal method for controlling the spread of the disease [5–8]. The COVID-19 outbreak has led to significant interest in developing robust mathematical models that can capture more complexities of the dynamics of disease transmission and control. Infectious disease models have proven to be essential tools in epidemiological research.

The findings of Daniel Bernoulli in the 18th century laid a strong foundation for the mathematical modelling of infectious diseases [9], and this research encouraged policymakers to adopt universal inoculation [10]. Modern mathematical modelling began in the 20th century [11–13]. In his research on malaria eradication, Ross [13] formulated a model to examine the threshold at which the mosquito population must be reduced to eliminate malaria. However, the work of Kermack [11, 12] became the foundation of modern mathematical modelling of infectious diseases with the formulation of the susceptible–infected–recovered (SIR) model. This model is useful in describing patterns in disease spread but can fail to capture the fine details required for some diseases. Over the years, this model has been adapted to incorporate more realistic scenarios that can more accurately capture the dynamics of infectious diseases.

Age structures have been widely used in infectious disease models to capture differences in disease susceptibility and contact patterns between age groups [14–17]. Kumar and Abbas [15] formulated an age-structured model to analyse infection transmission through direct contact (age-dependent mixing) and indirect contact (e.g. contaminated surfaces) using McKendrick–von Foerster partial differential equations (PDEs). Their model was formulated as an abstract semi-linear Cauchy problem, which allowed the authors to prove the existence of solutions and steady states. Chhetri *et al.* [18] used an age-structured model to study the COVID-19 transmission, vaccination, and control strategies. They analysed the model's positivity, boundedness, stability, and basic reproduction number R_0 using the next-generation matrix approach. Their numerical analysis considered various factors, including the effect of vaccination coverage and its efficacy in minimising infections and deaths. The age-structured PDE model proposed by Jing *et al.* [19] was used to study disease dynamics by incorporating vaccination and antiviral treatment as control measures. Their theoretical analysis proved the existence and stability of equilibria, showing that $R_0 < 1$ leads to eradication and $R_0 > 1$ leads to endemicity. However, substantial evidence indicates age-related disparities in susceptibility, severity, and mortality during the COVID-19 pandemic [16, 20, 21]. Davies *et al.* [16] found that individuals under 20 years of age are less susceptible, whereas O'Driscoll *et al.* [20] observed lower infection fatalities in the 5–9 age group than in the older groups. The age-structured model by Hilton and Keeling [22] estimates a country-specific basic reproduction number (R_0) and found that age and contact structures are crucial in COVID-19 transmission and that countries with older populations experienced a faster spread of the disease. The COVID-19 pandemic did not affect individuals and communities equally because individuals living in overcrowded conditions [23] and high-contact service occupations [24] were likely to be at a higher risk of infection than those who could work from home or live in a smaller family setting. This may increase the burden of

COVID-19 in socioeconomically disadvantaged communities. Therefore, a mathematical model is essential to examine the factors influencing disproportionate disease outcomes across deprivation deciles during the COVID-19 pandemic.

Several studies have attempted to understand the impact of confounding factors on infection outcomes [25–29]. For example, Hilton and Keeling [25] considered the combined effect of age and household structure on disease outcomes; Manna *et al.* [26, 27] developed a socioeconomic mixing matrix that combines age and other socioeconomic factors, such as income, employment, and level of education, to understand disease outcomes; and Hale *et al.* [29] used a stochastic compartmental infectious disease model that incorporates age and deprivation deciles using the Bayesian approach. The study by Munday *et al.* [30] was important for the development of the combined age and deprivation-decile mixing structure used in this study. Their model combines age and two risk groups (high and low) to understand the impact of vaccination on infectious disease (influenza and rubella) burdens. Although risk groups in disease modelling are useful, they are a "wide net" (meaning that different infections have different risk groups) when it comes to stratifying the population to understand infection outcomes.

This study presents a deterministic model that incorporates the confounding effects of age and deprivation-decile contact mixing, coupled with the time-dependent testing capacity of COVID-19. It uses POLYMOD age-mixing data [31] to quantify the age-mixing matrix and employs an equation [32] to quantify socially feasible types of mixing within and between deprivation deciles. We used analytical methods to analyse the equilibria and stability of the model. This study builds upon previous work by capturing how differences in both age and deprivation deciles, coupled with time-dependent testing capacity, influence disease transmission dynamics.

2 Mathematical Model Formulation

We consider an extended susceptible–exposed–infectious–recovered (SEIR) mathematical model of infectious diseases segregated into age groups $i = 1, \ldots, 21$ and deprivation deciles $n = 1, 2, \ldots, 10$. The model has eight epidemiological compartments: susceptible (S), exposed (E), asymptomatic (A), undetected symptomatic (J), detected symptomatic (I), hospitalised (H), recovered (R), and dead (D). Therefore, S_i^n is the number of susceptible individuals in age group i and deprivation decile n; the corresponding notation is used for all other compartments. Essentially, the model segments individuals based on both age and socioeconomic factors (as indicated by a deprivation decile) to better understand and predict disease dynamics within these compartments. The total population by age and deprivation decile is defined as

$$N_i^n = S_i^n + E_i^n + A_i^n + J_i^n + I_i^n + H_i^n + D_i^n + R_i^n. \tag{1}$$

In this model, as shown in Figure 1, susceptible individuals are infected after coming into contact with an infectious individual at a rate $\beta_i^n S_i^n / N_i^n$, which is a function of social mixing, age mixing, differential susceptibility, infectivity by age, and relative transmission. The exposed individuals transition to other compartments after a latency period σ and a time-varying testing fraction $\pi(t)$ divides them into either detected $\sigma\pi(t)E_i^n \to I_i^n$ or undetected $\sigma(1-\pi(t))E_i^n$. The undetected compartment was further subdivided into asymptomatic $\sigma(1-\pi(t))\rho E_i^n \to A_i^n$ and undetected symptomatic $\sigma(1-\pi(t))\theta E_i^n \to J_i^n$. Asymptomatic individuals recover at a rate γ, and symptomatic individuals J_i^n & I_i^n can recover or become hospitalised at rates γ and δ_i, respectively. Hospitalised individuals can either recover or die from infection at rates γ and d_i, respectively. We assumed that only hospitalised individuals died from the infection. We also assume that the test rate is a function of time because, at the start of an epidemic,

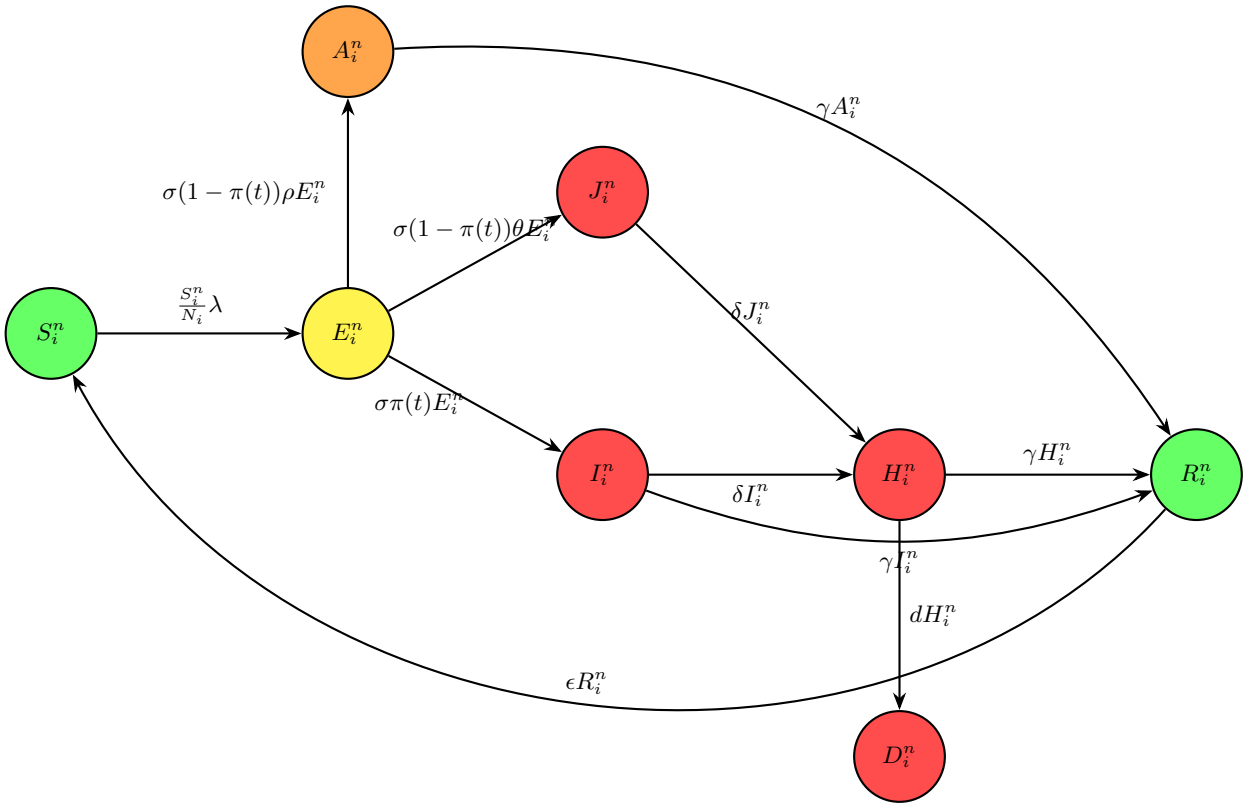

Fig 1. Schematic diagram of the epidemiological model of mixing within and between age groups and deprivation deciles. Susceptible individuals S_i^n (green) acquire an infection at the rate $\beta_i^n S_i^n / N_i^n$ and enter the latent class E_i^n (yellow). At rate σ, the exposed hosts are detected as symptomatic with a time-varying testing rate $\pi(t)$. Alternatively, at the rate $(1-\pi(t))$, they can enter the asymptomatic class A_i^n (orange) or the undetected symptomatic class J_i^n (red) in proportions ρ and θ. Asymptomatic, symptomatic, and hospitalised individuals recover to R_i^n(green) at the rate γ. Detected and undetected symptomatic individuals may become hospitalised H_i^n (red) at the rate δ_i.

the testing rate/capacity will be small compared to the later stages of the pandemic when testing is more readily available [36]. We defined the testing parameter $\pi(t)$ using the generalised Richards model (GRM) (extended logistic function) [37] *(see supplementary material).*

Key model assumptions

- The preferred mixing method ($\epsilon = 0.3$ in equation 5) was adopted for interactions between deprivation deciles, and it was assumed that similar age mixing [31] occurs consistently across these deciles.
- The age–deprivation contact matrix is held constant over the simulated period. This omits temporal changes in behaviour (lockdowns, school schedules, holidays) or adaptive responses to rising cases.
- Births, natural deaths, ageing between groups, and migration are ignored over the simulated periods, so population sizes in each compartment change only via

disease transitions.

- rate of recovery (γ), hospitalisation (δ_i), and death (d_i) are uniform across deciles. We assumed that deprivation affects only the contact rates.

2.1 Model Equations

The system of differential equations for the population in age group i and social group n is as follows:

$$\frac{dS_i^n}{dt} = -(\boldsymbol{\beta})_{i,n}(t)\frac{S_i^n}{N_i^n} + \epsilon R_i^n \tag{2a}$$

$$\frac{dE_i^n}{dt} = (\boldsymbol{\beta})_{i,n}(t)\frac{S_i^n}{N_i^n} - \sigma\left[\pi(t) + (1-\pi(t))\rho + (1-\pi(t))\theta\right]E_i^n \tag{2b}$$

$$\frac{dA_i^n}{dt} = \sigma(1-\pi(t))\rho E_i^n - \gamma A_i^n \tag{2c}$$

$$\frac{dJ_i^n}{dt} = \sigma(1-\pi(t))\theta E_i^n - \delta_i J_i^n - \gamma J_i^n \tag{2d}$$

$$\frac{dI_i^n}{dt} = \sigma\pi(t)E_i^n - \delta_i I_i^n - \gamma I_i^n \tag{2e}$$

$$\frac{dH_i^n}{dt} = \delta_i J_i^n + \delta_i I_i^n - \gamma H_i^n - d_i H_i^n \tag{2f}$$

$$\frac{dR_i^n}{dt} = \left(I_i^n + A_i^n + J_i^n + H_i^n\right)\gamma - \epsilon R_i^n \tag{2g}$$

$$\frac{dD_i^n}{dt} = d_i H_i^n \tag{2h}$$

where $\theta = 1-\rho$, and $\pi(t) + (1-\pi(t))\rho + (1-\pi(t))\theta = 1$. Here, $(\boldsymbol{\beta})_{i,n}(t)$ is defined as

$$(\boldsymbol{\beta})_{i,n}(t) = \sum_{k=1}^{10}\sum_{j=1}^{21}\boldsymbol{\lambda}_{i,n,j,k}\left(J_{j,k} + \iota I_{j,k} + A_{j,k}\right) \tag{3}$$

where $\boldsymbol{\lambda}_{i,n,j,k}$ is the contact rate between individuals in age group i and social group n and those in age group j and social group k as shown in Figure 2. Additionally, $\boldsymbol{\lambda}_{i,n,j,k}$ is the contact rate between individuals in age group i and social group n and those in age group j and social group k. Furthermore, $\boldsymbol{\lambda}_{i,n,j,k}$ are elements of the block matrix $\boldsymbol{\lambda}$, which is a square matrix of size $n \times n$, where $n = 1, 2, \ldots, 10$ and each element is a matrix of size $i, j = 1, 2, \ldots, 21$. In this model, we assume that only symptomatic and asymptomatic individuals $\mathbf{J}_{n,j}, \mathbf{I}_{n,j},$ and $, \mathbf{A}_{n,j}$ contribute directly to infection transmission, and that there is no transmission of infection in hospitals. In addition, we assume that asymptomatic individuals can transmit the disease without being aware of it, so we do not impose a modification factor for the transmission of asymptomatic individuals. In equation (3), we define

$$\boldsymbol{\lambda}_{i,n,j,k} = \hat{q}\left(w_{n,k}\cdot c_{i,j}\right), \tag{4}$$

where $\mathbf{C}$ is the age contact mixing matrix from the study of Mossong *et al.* [31], $\hat{q}$ is the relative transmission rate, and the social interaction by deprivation decile is derived using the method of Hethcote [32], being defined as

$$w_{n,m} = \left(\frac{\epsilon\nu_n\nu_m}{D} + \frac{(1-\epsilon)\nu_n\delta_{n,m}}{N_n}\right) \tag{5}$$

where $(\delta_{n,m} : m = m\ is\ 1,\ \&\ n \neq m\ is\ 0)$, $\epsilon \in [0,1]$, and ν_n are the average number of contacts for each sociodemographic group. Here, n and m are the deprivation deciles, N_n is the total population of each decile in England, $D = \Sigma_{n=1}\nu_n N_n$ is the total number of contacts per unit time for everyone in the population.

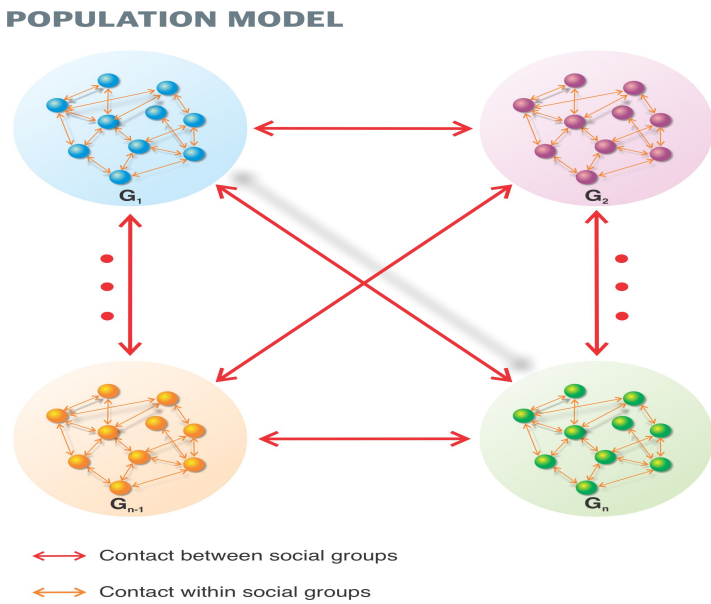

Fig 2. Population interactions by age and deprivation deciles. $G_1 \dots G_n$ are sociodemograhic groups which equate to deprivation deciles.

2.2 Basic Qualitative Properties of Model 2

In this subsection, we prove that the solution to system (2) is mathematically and biologically relevant if and only if it is positive and bounded.

Theorem 1 (Positivity)**.** *Let* $\Omega = \Big\{(S_i^n, E_i^n, A_i^n, J_i^n, I_i^n, H_i^n, R_i^n, D_i^n) \in \mathbb{R}_+^8 : N_i^n \leq \mathbf{N_0} : S_i^n(0) \geq 0, E_i^n(0) \geq 0, A_i^n(0) \geq 0, J_i^n(0) \geq 0, I_i^n(0) \geq 0, H_i^n(0) \geq 0, R_i^n(0) \geq 0, D_i^n(0) \geq 0\Big\}$. *Then, the solution* $(S_i^n(t), E_i^n(t), A_i^n(t), J_i^n(t), I_i^n(t), H_i^n(t), R_i^n(t), D_i^n(t))$ *of system (2) remains positive for all* $t > 0$.

Proof. The initial conditions $S_i^n(0) \geq 0, E_i^n(0) \geq 0, A_i^n(0) \geq 0, J_i^n(0) \geq 0, Q_i^n(0) \geq 0, I_i^n(0) \geq 0, H_i^n(0) \geq 0, R_i^n(0) \geq 0, D_i^n(0) \geq 0$ will be used to prove the positivity of the system (2). From equation (2a), we let

$$H = \frac{\beta_{n,i}}{N_i^n}, \tag{6}$$

Equation (2a) can now be written as

$$\frac{dS_i^n}{dt} + HS_i^n = \epsilon R_i^n. \tag{7}$$

The integrating factor of equation (7) is given by

$$\mathbf{IF} = e^{\int H ds}.$$

We multiply equation (7) by **IF**:

$$e^{\int_0^t H ds}\frac{dS_i^n}{dt} + e^{\int_0^t H ds} HS_i^n = \epsilon R_i^n \cdot e^{\int_0^t H ds}. \tag{8}$$

In equation (8), we observe that the LHS is the derivative of **IF** multiplied by S_i^n. Hence, we can write equation (8) as:

$$\frac{d}{dt}[e^{\int_0^t Hds} S_i^n] = \epsilon R_i^n \cdot e^{\int_0^t Hds}. \tag{9}$$

Taking the derivative of both sides, we obtain

$$\int_0^t \frac{d}{dt}\left(S_i^n(u) e^{\int_0^u Hds} S\right) du = \int_0^t \epsilon R(u) \cdot e^{\int_0^u Hds} du.$$

$$\implies S(t) e^{\int_0^t Hds} - S_i^n(0) = \int_0^t \epsilon R_i^n(u) \cdot e^{\int_0^u Hds} du.$$

Further rearranging yields

$$S_i^n(t) = S_i^n(0) \cdot e^{-\int_0^t Hds} + \int_0^t \epsilon R_i^n(u) \cdot e^{\int_u^t Hds} du. \tag{10}$$

From the initial conditions, we know that $S_i^n \geq 0$ means that $S_i^n(0) \cdot e^{-\int_0^t Hds} > 0$ and all parameters are positive. That is, $\epsilon > 0$, and hence, $\int_0^t \epsilon R_i^n(u) \cdot e^{\int_u^t Hds} du > 0$. Therefore, we can conclude that S_i^n is positive for all $t > 0$. The same is true for $E_i^n(0) \geq 0$, $A_i^n(0) \geq 0$, $J_i^n(0) \geq 0$, $Q_i^n(0) \geq 0$, $I_i^n(0) \geq 0$, $H_i^n(0) \geq 0$, $R_i^n(0) \geq 0$ and $D_i^n(0) \geq 0$.

□

Theorem 2 (boundedness)**.** *All feasible solutions of the model system (2) are uniformly bounded in a closed set* $\Omega = \left\{(S_i^n, E_i^n, A_i^n, J_i^n, I_i^n, H_i^n, R_i^n, D_i^n) \in \mathbb{R}_+^8 : N_i^n(0) \leq \mathbf{N_0}\right\}$.

Proof. At $t = 0$, $S_i^n(0) \geq 0$, $E_i^n(0) \geq 0$, $A_i^n(0) \geq 0$, $J_i^n(0) \geq 0$, $Q_i^n(0) \geq 0$, $I_i^n(0) \geq 0$, $H_i^n(0) \geq 0$, $R_i^n(0) \geq 0$, and $D_i^n(0) \geq 0$. Considering the boundedness of the system (2) under the initial conditions such that
$S_i^n(t) + E_i^n(t) + A_i^n(t) + J_i^n(t) + I_i^n(t) + H_i^n(t) + R_i^n(t) + D_i^n(t) = N_i^n(t)$, we have

$$\frac{dN_i^n}{dt} = \frac{dS_i^n}{dt} + \frac{dE_i^n}{dt} + \frac{dA_i^n}{dt} + \frac{dJ_i^n}{dt} + \frac{dI_i^n}{dt} + \frac{dH_i^n}{dt} + \frac{dR_i^n}{dt} + \frac{dD_i^n}{dt}.$$

By taking the sum of the system of ordinary differential equations, we obtain

$$\frac{dN_i^n}{dt} = 0.$$

This implies that N_i^n remains constant over time. By integrating both sides with respect to t and applying the initial condition $N_i^n(0) = \mathbf{N_0}$, we obtain $N_i^n(0) \leq \mathbf{N_0}$ for all t. Hence, the feasible solution of the model system remains in the region
$\Omega = \left\{(S_i^n, E_i^n, A_i^n, J_i^n, I_i^n, H_i^n, R_i^n, D_i^n) \in \mathbb{R}_+^8 : N_i^n(0) \leq \mathbf{N_0}\right\}$.

□

3 Presentation of the analytical result

We analysed our model analytically to verify whether the model system (2) behaves consistently with epidemiological intuition.

3.1 Disease-Free Equilibrium and Basic Reproduction Number

The basic reproduction number is the average number of infected individuals in a completely susceptible population. Considering the system of equations (2a–2h) and the total population in equation (1), the infected compartments are E_i^n (exposed), A_i^n (asymptomatic), J_i^n (undetected symptomatic), and I_i^n (detected symptomatic). The compartments A_i^n, J_i^n, and I_i^n contribute directly to the force of infection, whereas E_i^n is the point at which a susceptible individual comes into contact with an infected individual. In the disease-free equilibrium (DFE),
$E_i^n = A_i^n = J_i^n = I_i^n = H_i^n = D_i^n = R_i^n = 0$ and $S_i^n = N_i^n$.

We solve for R_0 using the next-generation matrix approach and then determine the dominant eigenvalue of $(\mathcal{T}\mathcal{V}^{-1})$. We divide the system into disease transmission $(\mathcal{T})$ and disease transition $(\mathcal{V}^{-1})$, as follows:

$$\mathcal{T} = \begin{bmatrix} \sum_{k=1}^{n}\sum_{j=1}^{i} \boldsymbol{\lambda}_{i,n,j,k}\left(\mathbf{J}_{n,j} + \iota\mathbf{I}_{n,j} + \mathbf{A}_{n,j}\right)\frac{S_i^n}{N_i^n} \\ 0 \\ 0 \\ 0 \\ 0 \end{bmatrix},$$

$$\mathcal{V} = \begin{bmatrix} \sigma E_i^n \\ -\sigma(1-\pi)\rho E_i^n + \gamma A_i^n \\ -\sigma(1-\pi)\theta E_i^n + (\delta_i+\gamma)J_i^n \\ -\sigma\pi E_i^n + (\delta_i+\gamma)I_i^n \end{bmatrix}.$$

The Jacobian of the two systems at the DFE and for $\theta = 1-\rho$ is calculated as

$$\mathcal{T} = \begin{bmatrix} 0 & \sum_{k=1}^{n}\sum_{j=1}^{i}\boldsymbol{\lambda}_{i,n,j,k} & \sum_{k=1}^{n}\sum_{j=1}^{i}\boldsymbol{\lambda}_{i,n,j,k} & \sum_{k=1}^{n}\sum_{j=1}^{i}\iota\boldsymbol{\lambda}_{i,n,j,k} \\ 0 & 0 & 0 & 0 \\ 0 & 0 & 0 & 0 \\ 0 & 0 & 0 & 0 \\ 0 & 0 & 0 & 0 \end{bmatrix}$$

$$\mathcal{V} = \begin{bmatrix} \sigma & 0 & 0 & 0 \\ -\sigma(1-\pi)\rho & \gamma & 0 & 0 \\ -\sigma(1-\pi)\theta & 0 & \delta_i+\gamma & 0 \\ -\sigma\pi & 0 & 0 & \delta_i+\gamma \end{bmatrix}.$$

The inverse of $\mathcal{V}$ is given by

$$\mathcal{V}^{-1} = \begin{bmatrix} \frac{1}{\sigma} & 0 & 0 & 0 \\ \frac{(1-\pi)\rho}{\gamma} & \frac{1}{\gamma} & 0 & 0 \\ \frac{(1-\pi)\theta}{\delta_i+\gamma} & 0 & \frac{1}{\delta_i+\gamma} & 0 \\ \frac{\pi}{\delta_i+\gamma} & 0 & 0 & \frac{1}{\delta_i+\gamma} \end{bmatrix}.$$

Hence, we can compute $\mathcal{T}\mathcal{V}^{-1}$ for one group as

$$\mathcal{T}\mathcal{V}^{-1} = \left[0, \boldsymbol{\lambda}_{n,j}\left(\frac{(1-\pi)\rho}{\gamma} + \frac{(1-\pi)\theta}{\delta_i+\gamma} + \frac{\iota\pi}{\delta_i+\gamma}\right), 0, 0\right]. \tag{11}$$

For multiple groups, we construct a full matrix

$$R_0 = \sum_{k=1}^{n}\sum_{j=1}^{i}\boldsymbol{\lambda}_{i,n,j,k}\left(\frac{(1-\pi)\rho}{\gamma} + \frac{(1-\pi)(1-\rho)}{\delta_j+\gamma} + \frac{\iota\pi}{\delta_j+\gamma}\right), \tag{12}$$

From equation (12), R_0 is largely dependent on the mixing matrix (which is the combination of age and deprivation mixing).

3.2 Stability of the Disease-Free Equilibrium

Theorem 3 (local stability)**.** *The DFE of system (2) is locally asymptotically stable (LAS) if $R_0 < 1$ and unstable if $R_0 > 1$.*

Proof. To demonstrate the local stability of our model, we linearise the system by finding the Jacobian at the DFE. The Jacobian matrix at the DFE, where $S_i^n = N_i^n$ and all other compartments are zero, is an 8×8 matrix

$$\mathbf{J} = \begin{pmatrix} 0 & 0 & -\beta^* & -\beta^* & -\iota\beta^* & 0 & \epsilon & 0 \\ 0 & -\sigma & \beta^* & \beta^* & \iota\beta^* & 0 & 0 & 0 \\ 0 & \sigma(1-\pi)\rho & -\gamma & 0 & 0 & 0 & 0 & 0 \\ 0 & \sigma(1-\pi)\theta & 0 & -(\delta_i+\gamma) & 0 & 0 & 0 & 0 \\ 0 & \sigma\pi & 0 & 0 & -(\delta_i+\gamma) & 0 & 0 & 0 \\ 0 & 0 & 0 & \delta_i & \delta_i & -(\gamma+d_i) & 0 & 0 \\ 0 & 0 & \gamma & \gamma & \gamma & \gamma & -\epsilon & 0 \\ 0 & 0 & 0 & 0 & 0 & d_i & 0 & 0 \end{pmatrix}. \tag{13}$$

For simplicity, let $\beta^* = \sum_{k=1}^{10}\sum_{j=1}^{21} \boldsymbol{\lambda}_{i,n,j,k}$. In this Jacobian matrix, the only nonzero entries in the first and last rows are ϵ and d_i, representing the rates at which individuals lose their immunity to become susceptible and die from a severe infection, respectively. These rates are negligible at DFE, as there are no infections, recoveries, or disease-related deaths. This implies that the impact of susceptibility loss due to infection exposure and infection-related death on the dynamics of other compartments is minimal. Hence, we focus on disease dynamics by removing the S_i^n and D_i^n compartments and reducing the system to six compartments: E_i^n, A_i^n, J_i^n, I_i^n, H_i^n, and R_i^n. The differential equations for these compartments at DFE are

$$\mathbf{J} = \begin{pmatrix} -\sigma & \beta^* & \beta^* & \iota\beta^* & 0 & 0 \\ \sigma(1-\pi)\rho & -\gamma & 0 & 0 & 0 & 0 \\ \sigma(1-\pi)\theta & 0 & -\delta_i-\gamma & 0 & 0 & 0 \\ \sigma\pi & 0 & 0 & -(\delta_i+\gamma) & 0 & 0 \\ 0 & 0 & \delta_i & \delta_i & -\gamma-d_i & 0 \\ 0 & \gamma & \gamma & \gamma & \gamma & -\epsilon \end{pmatrix}. \tag{14}$$

We obtain the characteristic equation by setting $|J - \lambda I|$ to zero:

$$|J-\lambda I| = \begin{vmatrix} -\sigma-\lambda & \beta^* & \beta^* & \iota\beta^* & 0 & 0 \\ \sigma(1-\pi)\rho & -\gamma-\lambda & 0 & 0 & 0 & 0 \\ \sigma(1-\pi)\theta & 0 & -\delta_i-\gamma-\lambda & 0 & 0 & 0 \\ \sigma\pi & 0 & 0 & -\delta_i-\gamma-\lambda & 0 & 0 \\ 0 & 0 & \delta_i & \delta_i & -\gamma-d_i-\lambda & 0 \\ 0 & \gamma & \gamma & \gamma & \gamma & -\epsilon-\lambda \end{vmatrix} = 0. \tag{15}$$

Hence, the coefficient of the characteristic polynomial is given by

$$\mathbf{F}(\lambda) = \lambda^7 + a_6\lambda^6 + a_5\lambda^5 + a_4\lambda^4 + a_3\lambda^3 + a_2\lambda^2 + a\lambda + a_0 = 0 \tag{16}$$

where

$$a_6 = 1$$

$$a_5 = \sigma + 4\gamma + 2\delta_i + d_i + \epsilon$$

$$\begin{aligned} a_4 =& 7\gamma^2 + 8\gamma\delta_i + 4\sigma\gamma + 3\sigma\delta_i + \delta_i^2 + 3d_i\delta_i + 3\epsilon\delta_i + \sigma d_i + 3\gamma d_i + \sigma\epsilon + 4\gamma\epsilon + 2d_i\epsilon \\ & - \lambda_{n,i}\sigma(1-\pi)\rho - \lambda_{n,i}\sigma(1-\pi)(1-\rho) - \iota\lambda_{n,i}\sigma\pi \end{aligned}$$

$$
\begin{aligned}
a_3 =& 4\gamma^3 + (6\epsilon + 6\sigma + 3d_i + \delta_i)\gamma^2 + 5\gamma^2\delta_i + (4\epsilon + 6\sigma + d_i)\gamma\delta_i + 2\gamma\delta_i^2 \\
&+ (2\epsilon + 3\sigma + 2d_i + 2\delta_i)\sigma\gamma + (2\epsilon + 2\sigma + d_i)d_i\delta_i + (\epsilon + \sigma + d_i)\delta_i^2 + (\epsilon + \sigma)d_i\sigma + \epsilon\sigma\delta_i \\
&- \sigma\lambda_{n,i}\left[(1-\pi)\rho(\epsilon + 3\gamma + d_i + 2\delta_i) + (1-\pi)(1-\rho)(\epsilon + 3\gamma + d_i + \delta_i) + \iota\pi(\epsilon + 3\gamma + d_i + \delta_i)\right]
\end{aligned}
$$

$$
\begin{aligned}
a_2 =& 6\gamma^4 + 11\gamma^3\delta_i + (6\sigma + 3d_i + 2\epsilon)\gamma^3 + (8\sigma + 4d_i + 5\epsilon + 2\delta_i)\gamma^2\delta_i + (4\sigma + 2d_i + \epsilon + \delta_i)\gamma\delta_i^2 + (d_i + \epsilon)\delta_i^3 \\
&+ (6\epsilon\sigma + 4\sigma^2 + 4\sigma d_i + 2\sigma\delta_i + 2\epsilon d_i + \epsilon\delta_i)\gamma^2 + (4\epsilon\sigma + 2\sigma^2 + 3\sigma d_i + 3\sigma\delta_i + \epsilon d_i)\gamma\delta_i \\
&+ (\sigma^2 + \sigma d_i + \sigma\delta_i)d_i\delta_i + (\sigma d_i + \sigma\delta_i)\delta_i^2 + (\epsilon\sigma + \sigma^2)d_i^2 + \epsilon\sigma^2\gamma + \epsilon\sigma\delta_i^2 \\
&- \sigma\lambda_{n,i}\big[(1-\pi)\rho(5\gamma^2 + 5\gamma\delta_i + 2d_i\gamma + 2d_i\delta_i + 2\epsilon\gamma + \epsilon d_i + \epsilon\delta_i) \\
&+(1-\pi)(1-\rho)(3\gamma^2 + 2\gamma\delta_i + d_i\gamma + d_i\delta_i + 2\epsilon\gamma + \epsilon d_i + \epsilon\delta_i) \\
&+\iota\pi(3\gamma^2 + 2\gamma\delta_i + d_i\gamma + d_i\delta_i + 2\epsilon\gamma + \epsilon d_i + \epsilon\delta_i)\big]
\end{aligned}
$$

$$
\begin{aligned}
a_1 =& 2\epsilon\gamma^4 + (5\epsilon + 2\sigma)\gamma^3\delta_i + (2\epsilon\sigma + 2\sigma^2 + 2\sigma d_i)\gamma^3 + (2\epsilon\sigma + 2\sigma d_i + 2\sigma\delta_i + \epsilon d_i + 2\epsilon\delta_i)\gamma^2\delta_i \\
&+ (\sigma d_i + \sigma\delta_i + \epsilon\delta_i)\gamma\delta_i^2 + \sigma d_i\delta_i^2 + (\sigma^2 + \sigma d_i + \sigma\delta_i)\epsilon\gamma^2 + (\sigma^2 + \sigma d_i)\epsilon\gamma\delta_i \\
&+ \sigma^2\epsilon d_i\gamma + \sigma^2\epsilon d_i\delta_i + \epsilon\sigma d_i^2\delta_i \\
&- \sigma\lambda_{n,i}\left[(1-\pi)\rho(\epsilon\gamma^2 + \epsilon\gamma\delta_i + \epsilon d_i\gamma + \epsilon d_i\delta_i + 2\sigma\gamma^2 + \sigma\gamma\delta_i)\right. \\
&\left.+(1-\pi)(1-\rho)(\epsilon\gamma^2 + \sigma\gamma^2 + \sigma\gamma\delta_i) + \iota\pi(\epsilon\gamma^2 + \sigma\gamma^2 + \sigma\gamma\delta_i)\right]
\end{aligned}
$$

$$
\begin{aligned}
a_0 =& \epsilon(\gamma + d_i)\left[\sigma\gamma(\delta_i + \gamma)^2 + \lambda_{n,i}\sigma(1-\pi)\rho(\delta_i + \gamma)^2\right. \\
&\left.-\lambda_{n,i}\sigma(1-\pi)(1-\rho)\gamma(\delta_i + \gamma) + \iota\lambda_{n,i}\sigma\pi\gamma(\delta_i + \gamma)\right].
\end{aligned}
$$

According to the Routh–Hurwitz condition, for $R_0 < 1$, the DFE is locally asymptotically stable if $a_6 > 0$, $a_5 > 0$, $a_4 > 0$, $a_3 > 0$, $a_2 > 0$, $a_1 > 0$, and $a_0 > 0$. That is,

$$a_6 = 1 > 0$$

$$a_5 = \sigma + 4\gamma + 2\delta_i + d_i + \epsilon > 0$$

$$
\begin{aligned}
a_4 =& 7\gamma^2 + 8\gamma\delta_i + 4\sigma\gamma + 3\sigma\delta_i + \delta_i^2 + 3d_i\delta_i + 3\epsilon\delta_i + \sigma d_i + 3\gamma d_i + \sigma\epsilon + 4\gamma\epsilon + 2d_i\epsilon \\
&- \lambda_{n,i}\sigma(1-\pi)\rho - \lambda_{n,i}\sigma(1-\pi)(1-\rho) - \iota\lambda_{n,i}\sigma\pi > 0
\end{aligned}
$$

$$
\begin{aligned}
a_3 =& 4\gamma^3 + (6\epsilon + 6\sigma + 3d_i + \delta_i)\gamma^2 + 5\gamma^2\delta_i + (4\epsilon + 6\sigma + d_i)\gamma\delta_i + 2\gamma\delta_i^2 \\
&+ (2\epsilon + 3\sigma + 2d_i + 2\delta_i)\sigma\gamma + (2\epsilon + 2\sigma + d_i)d_i\delta_i + (\epsilon + \sigma + d_i)\delta_i^2 + (\epsilon + \sigma)d_i\sigma + \epsilon\sigma\delta_i \\
&- \sigma\lambda_{n,i}\left[(1-\pi)\rho(\epsilon + 3\gamma + d_i + 2\delta_i) + (1-\pi)(1-\rho)(\epsilon + 3\gamma + d_i + \delta_i) + \iota\pi(\epsilon + 3\gamma + d_i + \delta_i)\right] > 0
\end{aligned}
$$

$$
\begin{aligned}
a_2 =& 6\gamma^4 + 11\gamma^3\delta_i + (6\sigma + 3d_i + 2\epsilon)\gamma^3 + (8\sigma + 4d_i + 5\epsilon + 2\delta_i)\gamma^2\delta_i + (4\sigma + 2d_i + \epsilon + \delta_i)\gamma\delta_i^2 + (d_i + \epsilon)\delta_i^3 \\
&+ (6\epsilon\sigma + 4\sigma^2 + 4\sigma d_i + 2\sigma\delta_i + 2\epsilon d_i + \epsilon\delta_i)\gamma^2 + (4\epsilon\sigma + 2\sigma^2 + 3\sigma d_i + 3\sigma\delta_i + \epsilon d_i)\gamma\delta_i \\
&+ (\sigma^2 + \sigma d_i + \sigma\delta_i)d_i\delta_i + (\sigma d_i + \sigma\delta_i)\delta_i^2 + (\epsilon\sigma + \sigma^2)d_i^2 + \epsilon\sigma^2\gamma + \epsilon\sigma\delta_i^2 \\
&- \sigma\lambda_{n,i}\big[(1-\pi)\rho(5\gamma^2 + 5\gamma\delta_i + 2d_i\gamma + 2d_i\delta_i + 2\epsilon\gamma + \epsilon d_i + \epsilon\delta_i) \\
&+(1-\pi)(1-\rho)(3\gamma^2 + 2\gamma\delta_i + d_i\gamma + d_i\delta_i + 2\epsilon\gamma + \epsilon d_i + \epsilon\delta_i) \\
&+\iota\pi(3\gamma^2 + 2\gamma\delta_i + d_i\gamma + d_i\delta_i + 2\epsilon\gamma + \epsilon d_i + \epsilon\delta_i)\big] > 0
\end{aligned}
$$

$$
\begin{aligned}
a_1 =& 2\epsilon\gamma^4 + (5\epsilon + 2\sigma)\gamma^3\delta_i + (2\epsilon\sigma + 2\sigma^2 + 2\sigma d_i)\gamma^3 + (2\epsilon\sigma + 2\sigma d_i + 2\sigma\delta_i + \epsilon d_i + 2\epsilon\delta_i)\gamma^2\delta_i \\
&+ (\sigma d_i + \sigma\delta_i + \epsilon\delta_i)\gamma\delta_i^2 + \sigma d_i\delta_i^2 + (\sigma^2 + \sigma d_i + \sigma\delta_i)\epsilon\gamma^2 + (\sigma^2 + \sigma d_i)\epsilon\gamma\delta_i \\
&+ \sigma^2\epsilon d_i\gamma + \sigma^2\epsilon d_i\delta_i + \epsilon\sigma d_i^2\delta_i \\
&- \sigma\lambda_{n,i}\left[(1-\pi)\rho(\epsilon\gamma^2 + \epsilon\gamma\delta_i + \epsilon d_i\gamma + \epsilon d_i\delta_i + 2\sigma\gamma^2 + \sigma\gamma\delta_i)\right. \\
&\left.+(1-\pi)(1-\rho)(\epsilon\gamma^2 + \sigma\gamma^2 + \sigma\gamma\delta_i) + \iota\pi(\epsilon\gamma^2 + \sigma\gamma^2 + \sigma\gamma\delta_i)\right] > 0
\end{aligned}
$$

$$
\begin{aligned}
a_0 =& \epsilon(\gamma + d_i)\left[\sigma\gamma(\delta_i + \gamma)^2 + \lambda_{n,i}\sigma(1-\pi)\rho(\delta_i + \gamma)^2\right. \\
&\left.+\iota\lambda_{n,i}\sigma\pi\gamma(\delta_i + \gamma)\right] - \left[(\lambda_{n,i}\sigma(1-\pi)(1-\rho)\gamma(\delta_i + \gamma))\,\epsilon(\gamma + d_i)\right](R_0 - 1).
\end{aligned}
$$

Thus, $a_0 > 0$ if $R_0 < 1$. Since all the coefficients are positive, we conclude that for $R_0 < 1$, the DFE point of our model is locally stable. □

Theorem 4 (global stability)**.** *The system (2) is globally asymptotically stable at the DFE if $R_0 < 1$ and unstable if $R_0 > 1$.*

Proof. Let us consider the Lyapunov function V of the form

$$V(t, E, A, J, I) = aE_i^n + bA_i^n + cJ_i^n + dI_i^n. \tag{17}$$

Its derivative is

$$\begin{aligned}\frac{dV}{dt} = a\Bigg[\sum_{k=1}^{n}\sum_{j=1}^{i}\boldsymbol{\lambda}_{i,n,j,k}\left(\mathbf{J}_{n,j} + \iota\mathbf{I}_{n,j} + \mathbf{A}_{n,j}\right)\frac{S_i^n}{N_i^n} - \sigma\left(((1-\pi)\rho + (1-\pi)(1-\rho) + \pi)\right)E_i^n\Bigg] \\ + \ b\left[\sigma(1-\pi)\rho E_i^n - \gamma A_i^n\right] + \ c\left[\sigma(1-\pi)(1-\rho)E_i^n - (\delta_i+\gamma)J_i^n\right] + d\left[\sigma\pi E_i^n - (\delta_i+\gamma)I_i^n\right].\end{aligned} \tag{18}$$

Rearranging such that like terms are collected together, and noting that at DFE, $S_i^n/N_i^n \leq 1$, we have

$$\begin{aligned}\frac{dV}{dt} \leq \ &\left[b\sigma(1-\pi)\rho + c\sigma(1-\pi)(1-\rho) + d\sigma\iota\pi - a\sigma\right]E_i^n + \left(a\sum_{k=1}^{n}\sum_{j=1}^{i}\boldsymbol{\lambda}_{i,n,j,k} - b\gamma\right)A_i^n \\ &+ \left(a\sum_{k=1}^{n}\sum_{j=1}^{i}\boldsymbol{\lambda}_{i,n,j,k} - c(\delta_i+\gamma)\right)J_i^n + \left(a\sum_{k=1}^{n}\sum_{j=1}^{i}\boldsymbol{\lambda}_{i,n,j,k} - d(\delta_i+\gamma)\right)I_i^n.\end{aligned} \tag{19}$$

Let $a = 1/\sigma$, $b = \sum_{k=1}^{n}\sum_{j=1}^{i}\boldsymbol{\lambda}_{i,n,j,k}/\gamma\sigma$, $c = \sum_{k=1}^{n}\sum_{j=1}^{i}\boldsymbol{\lambda}_{n,k}/(\delta_i+\gamma)\sigma$ and $d = \iota\sum_{k=1}^{n}\sum_{j=1}^{i}\boldsymbol{\lambda}_{n,k}/(\delta_i+\gamma)\sigma$. Substituting these into equation (19) leads to

$$\frac{dV}{dt} \leq (R_0 - 1)E_i^n. \tag{20}$$

Hence, $\frac{dV}{dt} \leq (R_0 - 1)E_i^n$; it is important to note that $\frac{dV}{dt} = 0$ only at DFE. From LaSalle's invariance principle, it follows that all solutions of equation (2) converge to the DFE as $t \to \infty$ whenever $R_0 < 1$. The DFE is globally asymptotically stable when $R_0 < 1$. □

3.3 Existence of an Endemic Equilibrium Point

We calculate the endemic equilibrium by equating the system (2) to zero; then, we obtain $E_1 = (S_i^{n*}, E_i^{n*}, A_i^{n*}, J_i^{n*}, Q_i^{n*}, I_i^{n*}, H_i^{n*}, R_i^{n*}, D_i^{n*})$, such that

$$S_i^{n*} = \frac{\epsilon R_i^{n*}}{H^{**}} \tag{21a}$$

$$E_i^{n*} = \frac{H^{**} S_i^{n*}}{\sigma} \tag{21b}$$

$$A_i^{n*} = \frac{\sigma(1-\pi)\rho E_i^{n*}}{\gamma} \tag{21c}$$

$$J_i^{n*} = \frac{\sigma(1-\pi)\theta E_i^{n*}}{(\delta_i+\gamma)} \tag{21d}$$

$$I_i^{n*} = \frac{\sigma\pi E_i^{n*}}{(\delta_i+\gamma)} \tag{21e}$$

$$H_i^{n*} = \frac{\delta_i\sigma}{(\delta_i+d_i)(\delta_i+\gamma)}\left[(1-\pi)\theta+\pi\right] E_i^{n*} \tag{21f}$$

$$R_i^{n*} = \frac{\gamma}{\epsilon}\left[I_i^{n*} + A_i^{n*} + J_i^{n*} + H_i^{n*}\right]. \tag{21g}$$

From equation (6), we define

$$H^{**} = \sum_{k=1}^{n}\sum_{j=1}^{i} \frac{\boldsymbol{\lambda}_{i,n,j,k}}{N_i^n}\left(\mathbf{J}_{k,j} + \iota\mathbf{I}_{k,j} + \mathbf{A}_{k,j}\right). \tag{22}$$

At endemic equilibrium, we know that $H_i^{n*} \geq 0$ and that all our parameters are positive, so $d_i \neq 0$. We can conclude that D_i^{n*} depends on H_i^{n*}.

3.3.1 Uniqueness of the Endemic Equilibrium Point

Theorem 5. *An endemic equilibrium is unique iff $R_0 > 1$.*

Proof. If we rewrite equations (21c–21g) in terms of equation (21b), we have

$$A_i^{n*} = \frac{(1-\pi)\rho H^{**} S_i^{n*}}{\gamma} \tag{23a}$$

$$J_i^{n*} = \frac{(1-\pi)\theta H^{**} S_i^{n*}}{(\delta_i+\gamma)} \tag{23b}$$

$$I_i^{n*} = \frac{\pi H^{**} S_i^{n*}}{(\delta_i+\gamma)} \tag{23c}$$

$$H_i^{n*} = \frac{\delta_i}{(\delta_i+d_i)(\delta_i+\gamma)}\left[(1-\pi)\theta+\pi\right] H^{**} S_i^{n*}. \tag{23d}$$

Substituting A_i^{n*}, J_i^{n*}, I_i^{n*}, and H_i^{n*} from equations (23a–23d) into (21g), we obtain

$$R_i^{n*} = \frac{\gamma}{\epsilon}\left(\frac{(1-\pi)\rho H^{**} S_i^{n*}}{\gamma} + \frac{(1-\pi)\theta H^{**} S_i^{n*}}{(\delta_i+\gamma)} + \frac{\pi H^{**} S_i^{n*}}{(\delta_i+\gamma)} + \nu_1 H^{**} S_i^{n*}\Big)\right) \tag{24}$$

where

$$\nu_1 = \frac{\delta_i}{(\delta_i+d_i)(\delta_i+\gamma)}\left[(1-\pi)\theta+\pi\right].$$

Equation (22) implies that

$$H^{**} N_i^{n*} = \sum_{k=1}^{n}\sum_{j=1}^{i} \boldsymbol{\lambda}_{i,n,j,k}\left(\mathbf{J}_{k,j}^* + \iota\mathbf{I}_{k,j}^* + \mathbf{A}_{k,j}^*\right), \tag{25}$$

which implies that

$$H^{**}P_2 = \sum_{k=1}^{n}\sum_{j=1}^{i} \boldsymbol{\lambda}_{i,n,j,k}\left(\frac{(1-\pi)\rho H^{**}S_i^{n*}}{\gamma} + \frac{(1-\pi)\theta H^{**}S_i^{n*}}{(\delta_i+\gamma)} + \iota\frac{\pi H^{**}S_i^{n*}}{(\delta_i+\gamma)}\right). \quad (26)$$

P_2 is derived from $N_i^{n*} = S_i^{n*} + E_i^{n*} + A_i^{n*} + J_i^{n*} + I_i^{n*} + H_i^{n*} + R_i^{n*} + D_i^{n*}$. Dividing both sides of equation (26) by $H^{**}S_i^{n*}$, we have

$$1 + P_3H^{**} = R_0. \quad (27)$$

Solving for H^{**} in equation (27), we have

$$H^{**} = \frac{R_0 - 1}{P_3} \quad (28)$$

and $P_3 > 0$. Here, P_3 is defined as

$$\frac{\mathbf{K} + \frac{1}{\sigma} + \nu_2}{\gamma\mathbf{K}},$$

Where $\mathbf{K} = \left(\frac{(1-\pi)\rho}{\gamma} + \frac{(1-\pi)\theta}{(\delta_i+\gamma)} + \frac{\pi}{(\delta_i+\gamma)} + \nu_1\right)$, and $\nu_2 = \frac{\gamma}{\epsilon}\left(\frac{(1-\pi)\rho}{\gamma} + \frac{(1-\pi)\theta}{(\delta_i+\gamma)} + \frac{\pi}{(\delta_i+\gamma)} + \nu_1\right)$. All parameters are positive; hence, $\gamma > 0$ and $\mathbf{K} > 0$, so $\gamma\mathbf{K} > 0$. Therefore, $H^{**} > 0$ iff $R_0 > 1$. Therefore, a unique endemic equilibrium exists. □

3.4 Global Stability of the Endemic Equilibrium

Theorem 6 (global stability of endemic equilibrium)**.** *The endemic equilibrium E_1 of the model system (2) is globally asymptotically stable if $R_0 > 1$.*

Proof. To prove global stability, we used the Lyapunov function method. Consider the Lyapunov function of the form

$$L = \left(S_i^n - S_i^{n*} - S_i^{n*}\log\frac{S_i^n}{S_i^{n*}}\right) + \left(E_i^n - E_i^{n*} - E_i^{n*}\log\frac{E_i^n}{E_i^{n*}}\right) + \left(A_i^n - A_i^{n*} - A_i^{n*}\log\frac{A_i^n}{A_i^{n*}}\right) + \left(J_i^n - J_i^{n*} - J_i^{n*}\log\frac{J_i^n}{J_i^{n*}}\right)$$
$$+ \left(I_i^n - I_i^{n*} - I_i^{n*}\log\frac{I_i^n}{I_i^{n*}}\right) + \left(H_i^n - H_i^{n*} - H_i^{n*}\log\frac{H_i^n}{H_i^{n*}}\right) + \left(R_i^n - R_i^{n*} - R_i^{n*}\log\frac{R_i^n}{R_i^{n*}}\right) + \left(D_i^n - D_i^{n*} - D_i^{n*}\log\frac{D_i^n}{D_i^{n*}}\right).$$

Taking the derivative of L, we obtain

$$\frac{dL}{dt} = \left(\frac{S_i^n - S_i^{n*}}{S_i^n}\right)\frac{dS_i^n}{dt} + \left(\frac{E_i^n - E_i^{n*}}{E_i^n}\right)\frac{dE_i^n}{dt} + \left(\frac{A_i^n - A_i^{n*}}{A_i^n}\right)\frac{dA_i^n}{dt} + \left(\frac{J_i^n - J_i^{n*}}{J_i^n}\right)\frac{dJ_i^n}{dt} + \left(\frac{I_i^n - I_i^{n*}}{I_i^n}\right)\frac{dI_i^n}{dt}$$
$$+ \left(\frac{H_i^n - H_i^{n*}}{H_i^n}\right)\frac{dH_i^n}{dt} + \left(\frac{R_i^n - R_i^{n*}}{R_i^n}\right)\frac{dR_i^n}{dt} + \left(\frac{D_i^n - D_i^{n*}}{D_i^n}\right)\frac{dD_i^n}{dt}. \quad (29)$$

Substituting the value of the derivatives into (29) yields

$$\frac{dL}{dt} = \left(\frac{S_i^n - S_i^{n*}}{S_i^n}\right)\left[-(\boldsymbol{\beta})_{n,i}(t)\frac{S_i^n}{N_i^n} + \epsilon R_i^n\right] + \left(\frac{E_i^n - E_i^{n*}}{E_i^n}\right)\left[(\boldsymbol{\beta})_{n,i}(t)\frac{S_i^n}{N_i^n} - \sigma E_i^n\right] + \left(\frac{A_i^n - A_i^{n*}}{A_i^n}\right)\left[\sigma\left(1-\pi(t)\right)\rho E_i^n - \gamma A_i^n\right]$$
$$+ \left(\frac{J_i^n - J_i^{n*}}{J_i^n}\right)\left[\sigma(1-\pi(t))\theta E_i^n - \delta_i J_i^n - \gamma J_i^n\right] + \left(\frac{I_i^n - I_i^{n*}}{I_i^n}\right)\left[\sigma\pi E_i^n - \delta_i I_i^n - \gamma I_i^n\right]$$
$$+ \left(\frac{H_i^n - H_i^{n*}}{H_i^n}\right)\left[\delta_i J_i^n + \delta_i I_i^n - \gamma H_i^n - d_i H_i^n\right] + \left(\frac{R_i^n - R_i^{n*}}{R_i^n}\right)\left[\left(I_i^n + A_i^n + J_i^n + H_i^n\right)\gamma - \epsilon R_i^n\right]$$
$$+ \left(\frac{D_i^n - D_i^{n*}}{D_i^n}\right) d_i H_i^n.$$

By substituting $(\beta)_{n,i}$, we obtain

$$
\begin{aligned}
\frac{dL}{dt} = \frac{S_i^n - S_i^{n*}}{S_i^n} & \left[- \frac{\sum_{k=1}^{n}\sum_{j=1}^{i} \boldsymbol{\lambda}_{i,n,j,k}}{N_i^n} \Big((J_i^n - J_i^{n*})(S_i^n - S_i^{n*}) + \iota\,(I_i^n - I_i^{n*})(S_i^n - S_i^{n*}) + (A_i^n - A_i^{n*})(S_i^n - S_i^{n*}) \Big) + \epsilon\,(R_i^n - R_i^{n*}) \right] \\
& + \frac{E_i^n - E_i^{n*}}{E_i^n} \left[\frac{\sum_{k=1}^{n}\sum_{j=1}^{i} \boldsymbol{\lambda}_{i,n,j,k}}{N_i^n} \Big((J_i^n - J_i^{n*})(S_i^n - S_i^{n*}) + \iota\,(I_i^n - I_i^{n*})(S_i^n - S_i^{n*}) + (A_i^n - A_i^{n*})(S_i^n - S_i^{n*}) \Big) - (E_i^n - E_i^n) \right] \\
& + \frac{A_i^n - A_i^{n*}}{A_i^n} \left[\sigma\,(1 - \pi(t))\,\rho\,E_i^n \; - \; \gamma\,A_i^n \right] \\
& + \frac{J_i^n - J_i^{n*}}{J_i^n} \left[\sigma\,(1 - \pi(t))\,\theta\,E_i^n \; - \; (\delta_i + \gamma)\,J_i^n \right] \\
& + \frac{I_i^n - I_i^{n*}}{I_i^n} \left[\sigma\,\pi\,E_i^n \; - \; (\delta_i + \gamma)\,I_i^n \right] \\
& + \frac{H_i^n - H_i^{n*}}{H_i^n} \left[\delta_i\,(J_i^n + I_i^n) \; - \; (\gamma + d_i)\,H_i^n \right] \\
& + \frac{R_i^n - R_i^{n*}}{R_i^n} \left[\gamma\,(I_i^n + A_i^n + J_i^n + H_i^n) \; - \; \epsilon\,R_i^n \right] \\
& + \frac{D_i^n - D_i^{n*}}{D_i^n}\; d_i\,H_i^n\,. \qquad (30)
\end{aligned}
$$

After some algebra, it is possible to split equation (30) into positive and negative parts:

$$
\begin{aligned}
\frac{dL^+}{dt} = & \frac{S_i^n - S_i^{n*}}{S_i^n}\;\epsilon\,(R_i^n - R_i^{n*}) \\
& + \frac{E_i^n - E_i^{n*}}{E_i^n}\;\frac{\sum_{k=1}^{n}\sum_{j=1}^{i} \boldsymbol{\lambda}_{i,n,j,k}}{N_i^n} \Big[(J_i^n - J_i^{n*})(S_i^n - S_i^{n*}) + \iota\,(I_i^n - I_i^{n*})(S_i^n - S_i^{n*}) + (A_i^n - A_i^{n*})(S_i^n - S_i^{n*}) \Big] \\
& + \frac{A_i^n - A_i^{n*}}{A_i^n} \left[\sigma(1 - \pi(t))\,\rho\,E_i^n \; - \; \gamma\,A_i^n \right] \\
& + \frac{J_i^n - J_i^{n*}}{J_i^n} \left[\sigma(1 - \pi(t))\,\theta\,E_i^n \; - \; (\delta_i + \gamma)\,J_i^n \right] \\
& + \frac{I_i^n - I_i^{n*}}{I_i^n} \left[\sigma\,\pi\,E_i^n \; - \; (\delta_i + \gamma)\,I_i^n \right] \\
& + \frac{H_i^n - H_i^{n*}}{H_i^n} \left[\delta_i\,(J_i^n + I_i^n) \; - \; (\gamma + d_i)\,H_i^n \right] \\
& + \frac{R_i^n - R_i^{n*}}{R_i^n} \left[\gamma\,(I_i^n + A_i^n + J_i^n + H_i^n) \; - \; \epsilon\,R_i^n \right] \\
& + \frac{D_i^n - D_i^{n*}}{D_i^n}\; d_i\,H_i^n\,. \qquad (31)
\end{aligned}
$$

Taking the positive terms, we have

$$\begin{aligned}\frac{dL^+}{dt} =& \frac{(S_i^n - S_i^{n*})^2}{S_i^n} \frac{\sum_{k=1}^{n}\sum_{j=1}^{i} \boldsymbol{\lambda}_{i,n,j,k}}{N_i^n} [J_i^{n*} + I_i^{n*} + A_i^{n*}] + \frac{(S_i^n - S_i^{n*})}{S_i^n} \epsilon R_i^n \\ &+ \frac{(E_i^n - E_i^{n*})}{E_i^n} \frac{\sum_{k=1}^{n}\sum_{j=1}^{i} \boldsymbol{\lambda}_{i,n,j,k}}{N_i^n} [I_i^n S_i^n + I_i^{n*} S_i^{n*} + A_i^n S_i^n + A_i^{n*} S_i^{n*} + J_i^n S_i^n + J_i^{n*} S_i^{n*}] + \frac{(A_i^n - A_i^{n*})}{A_i^n} [\sigma\rho E_i^n + \sigma\pi\rho E_i^{n*}] \\ &+ \frac{(J_i^n - J_i^{n*})}{J_i^n} [\sigma\theta E_i^n + \sigma\pi\theta E_i^{n*}] + \frac{(I_i^n - I_i^{n*})}{I_i^n} [\sigma\pi E_i^n] + \frac{(H_i^n - H_i^{n*})}{H_i^n} [\delta_i I_i^n + \delta_i J_i^n] \\ &+ \frac{(R_i^n - R_i^{n*})}{R_i^n} [\gamma I_i^n + \gamma A_i^n + \gamma J_i^n + \gamma H_i^n] + \frac{(D_i^n - D_i^{n*})}{D_i^n} d_i H_i^n. \end{aligned} \tag{32}$$

Taking the negative terms, we have

$$\begin{aligned}\frac{dL^-}{dt} =& -\left(\frac{(S_i^n - S_i^{n*})^2}{S_i^n} \frac{\sum_{k=1}^{n}\sum_{j=1}^{i} \boldsymbol{\lambda}_{i,n,j,k}}{N_i^n} [J_i^n + I_i^n + A_i^n] \right) - \frac{(S_i^n - S_i^{n*})}{S_i^n} \epsilon R_i^{n*} \\ &- \frac{(E_i^n - E_i^{n*})^2}{E_i^n} \sigma \left(\frac{E_i^n - E_i^{n*}}{E_i^n} \right) \frac{\sum_{k=1}^{n}\sum_{j=1}^{i} \boldsymbol{\lambda}_{i,n,j,k}}{N_i^n} [J_i^n S_i^{n*} + J_i^{n*} S_i^n + I_i^n S_i^{n*} + I_i^{n*} S_i^n + A_i^n S_i^{n*} + A_i^{n*} S_i^n] \\ &- \left(\frac{A_i^n - A_i^{n*}}{A_i^n} \right) [\sigma\pi\rho E_i^n + \sigma\pi\rho E_i^{n*}] - \left(\frac{J_i^n - J_i^{n*}}{J_i^n} \right) [\sigma E_i^{n*} + \sigma\rho E_i^n + \sigma\pi E_i^n \sigma\pi E_i^{n*}] - \left(\frac{I_i^n - I_i^{n*}}{I_i^n} \right) [\sigma\pi E_i^{n*}] \\ &- \left(\frac{H_i^n - H_i^{n*}}{H_i^n} \right) [\delta_i I_i^{n*} + \delta_i J_i^{n*}] \left(\frac{R_i^n - R_i^{n*}}{R_i^n} \right) [\gamma I_i^{n*} + \gamma J_i^{n*} + \gamma A_i^{n*} + \gamma H_i^{n*}] - \frac{(D_i^n - D_i^{n*})}{D_i^n} d_i H_i^{n*}. \end{aligned} \tag{33}$$

We can write $\frac{dL}{dt} = \mathbf{A} - \mathbf{B}$, where $\mathbf{A}$ represents the positive terms (32) and $\mathbf{B}$ the negative terms (33). Thus, if $\mathbf{A} < \mathbf{B}$, then we obtain that $\frac{dL}{dt} \leq 0$ iff $(S_i^n = S_i^{n*}, E_i^n = E_i^{n*}, A_i^n = A_i^{n*}, J_i^n = J_i^{n*}, I_i^n = I_i^{n*}, H_i^n = H_i^{n*}, R_i^n = R_i^{n*}, D_i^n = D_i^{n*})$. Therefore, the largest compact invariant set in $(S_i^{n*}, E_i^{n*}, A_i^{n*}, J_i^{n*}, I_i^{n*}, H_i^{n*}, R_i^{n*}, D_i^{n*}) \in \Omega : \frac{dL}{dt} = 0$ is the singleton set, E_{eff}, where E_{eff} is the endemic equilibrium of the system. According to LaSalle's invariance principle, this implies that E_1 is globally asymptotically stable in Ω if $\mathbf{A} < \mathbf{B}$. □

3.5 Sensitivity Analysis

We performed a sensitivity analysis to study how the uncertainty in the model output could be predicted by the uncertainty in the model input. This analysis helps the mathematical modeller validate their assumptions and improve trust in the results of the model. The normalised sensitivity index for each parameter X within R_0 is defined as

$$S_X^{R_0} = \frac{\partial R_0}{\partial X} \times \frac{X}{R_0},$$

which was used in studies by Wodajo *et al.* [38] and Al-arydah [39]. Parameters with a high sensitivity index have a greater influence on the R_0 value. The sign of the index indicates whether the parameter influences R_0 positively or negatively. From Figure 3, it can be seen that the contact rate, proportion of asymptomatic individuals in the population, testing rate, recovery rate, and rate of hospitalisation are the key

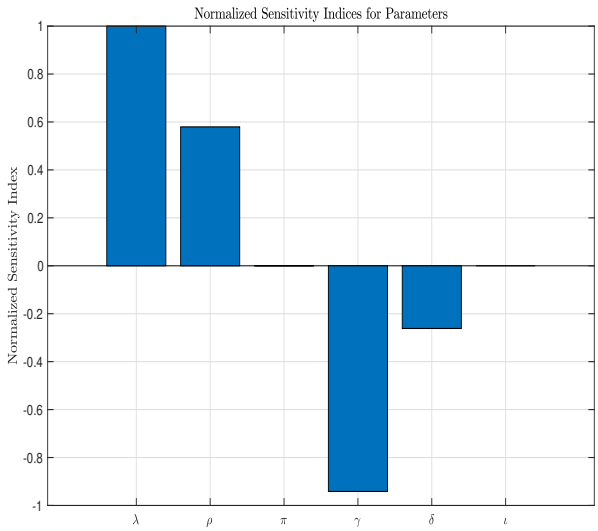

Fig 3. Bar chart of normalised sensitivity indices for key model parameters affecting the basic reproduction number R_0. Each bar represents the relative impact of changes in the model parameters, with positive values indicating parameters that increase R_0 and negative values indicating those that decrease it. High sensitivity values imply that small changes in these parameters can significantly affect the disease transmission. Key parameters include the contact rate λ, recovery rate γ, and hospitalisation rate δ.

parameters that influence the reproduction number, whereas the sensitivity of the test and average number of days for the test to be reported have a small influence.

The sensitivity indices were expressed as follows:

1. The sensitivity index for $\lambda_{i,n,j,k}$ is

$$\sum_{k=1}^{10}\sum_{j=1}^{21} S_{\lambda_{i,n,j,k}} = \frac{1}{R_0}\sum_{k=1}^{10}\sum_{j=1}^{21} \lambda_{i,n,j,k}\, A_j = \frac{R_0}{R_0} = 1\,,$$

   where $A_j = \frac{(1-\pi)\rho}{\gamma} + \frac{(1-\pi)(1-\rho)}{\delta_j+\gamma} + \frac{\iota\pi}{\delta_j+\gamma}$. This indicates that the normalised sensitivity index of $\lambda_{i,n,j,k}$ is a matrix of ones.

2. The sensitivity index for γ is

$$S_\gamma = \frac{1}{R_0}\sum_{k=1}^{10}\sum_{j=1}^{21} \lambda_{i,n,j,k}\left[-\frac{(1-\pi)\rho}{\gamma} - \frac{\gamma\left((1-\pi)(1-\rho)+\iota\pi\right)}{(\delta_j+\gamma)^2}\right]. \tag{34}$$

3. The sensitivity index for ρ is

$$S_\rho = \frac{\rho}{R_0}\sum_{k=1}^{10}\sum_{j=1}^{21} \lambda_{i,n,j,k}\left[\frac{1-\pi}{\gamma} - \frac{1-\pi}{\delta_j+\gamma}\right].$$

4. The sensitivity index for δ_j is

$$S_{\delta_j} = \frac{\delta_j}{R_0}\sum_{k=1}^{10}\sum_{j=1}^{21} \lambda_{i,n,j,k}\left[-\frac{(1-\pi)(1-\rho)+\iota\pi}{(\delta_j+\gamma)^2}\right].$$

However, we can compute the sensitivity index specific to each j by summing only over the index k. The normalised sensitivity index for δ_j is given by

$$S_{\delta_j} = \frac{\delta_j}{R_0} \sum_{k=1}^{10} \lambda_{i,n,j,k} \left[-\frac{(1-\pi)(1-\rho) + \iota\pi}{(\delta_j + \gamma)^2} \right].$$

5. The sensitivity index for π is

$$S_\pi = \frac{\pi}{R_0} \left(\sum_{k=1}^{10} \sum_{j=1}^{21} \lambda_{i,n,j,k} \left[-\frac{\rho}{\gamma} - \frac{1-\rho}{\delta_j + \gamma} + \frac{\iota}{\delta_j + \gamma} \right] \right). \tag{35}$$

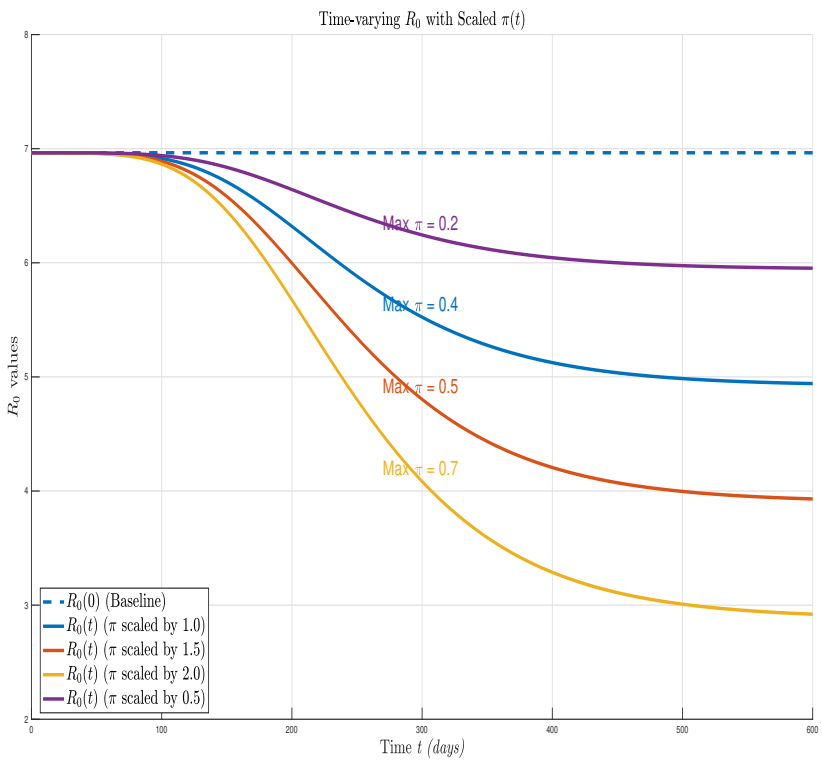

Fig 4. Time-varying basic reproduction number $R_0(t)$ under different testing rate trajectories $\pi(t)$. The dashed horizontal line marks the initial reproduction number $R_0(0) \approx 7.0$. Solid curves show how $R_0(t)$ declines as the cumulative testing capacity increases according to a logistic "generalized Richard" curve scaled by factors 0.5, 1.0, 1.5, and 2.0 (yielding maximum proportions of the testpopulation of 0.2, 0.4, 0.5, and 0.7, respectively). Increased testing reduces the proportion of undetected (and thus fully transmissible) infections, lowering R_0, but—even at the highest feasible testing scale—cannot on its own drive R_0 below 1.

6. The sensitivity index for ι is

$$S_\iota = \frac{\iota}{R_0} \sum_{k=1}^{10} \sum_{j=1}^{21} \lambda_{i,n,j,k} \frac{\pi}{\delta_j + \gamma}.$$

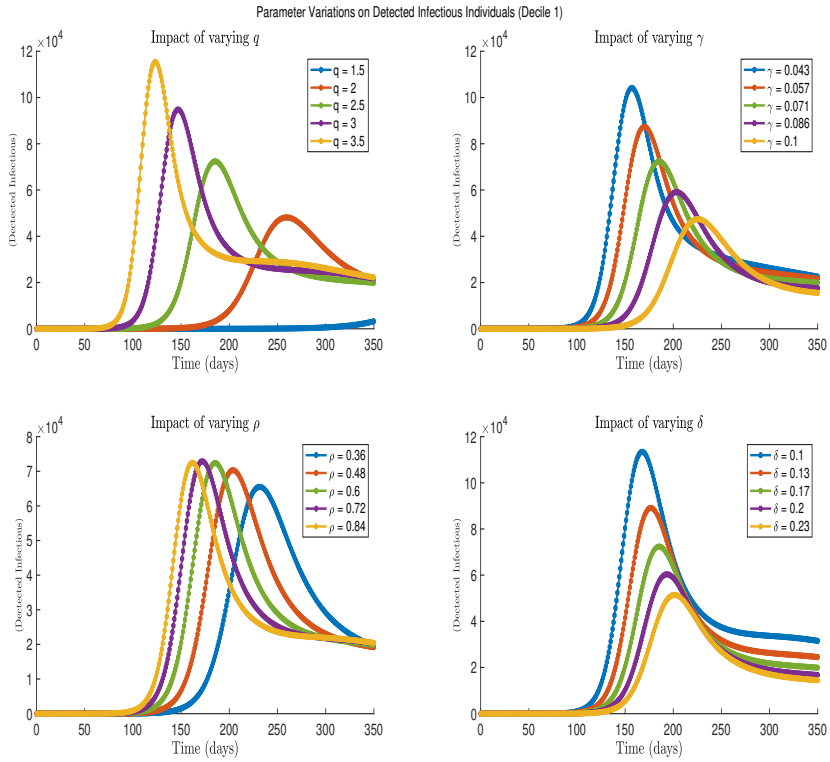

Fig 5. Sensitivity of infection dynamics in the most-deprived decile (Decile 1) when $R_0 > 1$. Each panel shows the time series of detected infectious individuals under $\pm 20\%$ variation from baseline values in some key parameters: relative transmission rate $\hat{q}$, proportion of asymptomatic ρ, recovery rate γ, and the rate of hospitalisation δ. Changes in these parameters can have a significant impact on the peak of infection.

4 Numerical Analysis

We numerically analysed the sensitivity indices associated with each parameter. Numerical analysis was performed in MATLAB using the built-in ode45 solver with the parameter values listed in Table 1. The initial conditions for each age group and deprivation decile were set such that the entire population was susceptible, except for a small seed of latent infections ($E^1_{15}(0) = 1$) to initiate spread. The parameter values were obtained from existing literature, except where otherwise stated. A sensitivity analysis was performed using the sensitivity index method and numerically by perturbing some of the parameters to observe their impact on the system dynamics, as presented in Figure 5. Under the baseline mixing patterns, relative transmission rate $\hat{q}$, and parameter values, the next-generation matrix approach yields a basic reproduction number of $R_0 = 3.34$. However, when we reduce the relative transmission rate $\hat{q}$ by 80%, the R_0 values decrease below 1, indicating that a reduction in the transmission rate, which directly affects the mixing and contact patterns, is sufficient to take R_0 below the threshold for sustained spread. Finally, Figures 6 and 7 illustrate the time courses of all compartments (susceptible, exposed, asymptomatic, infectious, hospitalised, recovered) aggregated over age for each of the ten deprivation deciles. It can be seen that the more deprived groups peaked earlier and attained higher burdens of infection and

hospitalisation.

Parameter	Description	Value and Source
$c_{i,j}$	Contact matrix by age	[31]
ι	Modification factor by which confirmed and reported individuals can transmit an infection.	0.6 (assumed)
ρ	Proportion of population who are asymptomatic	0.6
$\pi(t)$	Time-dependent fraction of exposures reported	fitted
$\hat{q}$	Relative transmission rate	2.5 (assumed)
γ	Recovery rate	1/14 days^{-1} [34]
δ_i	Rate at which symptomatic or positive quarantine individuals become sick and require hospital care, which varies by age	[33]
d_i	Rate at which hospitalised individuals become fatally sick, which varies by age	[33]
ϵ	Probability of waning immunity	2/100 $days^{-1}$ [35]
a_i	Infectivity by age	[33]
h_i	Susceptibility by age	[33]

Table 1. Parameter descriptions and values

4.1 Simulation of model (2) at $R_0 > 1$

In Figure 6, we plotted the full time series of the model's eight compartments (susceptible, exposed, asymptomatic, undetected, and detected symptomatic, hospitalised, recovered, and deceased) aggregated over age for each deprivation decile using the baseline parameter set (Table 1). Deciles1–10 are shown in separate panels, highlighting that the most-deprived groups experience earlier and larger infection peaks. In Figure 7, we focus on the breakdown of the infectious compartments, again summed over age within each decile, and using the baseline parameter set (Table 1).

4.2 Pairwise variation of key epidemiological parameters

In Figure 8, we hold the age–deprivation contact matrix fixed and compute R_0 across a $\pm 20\%$ grid of the relative transmission rate $\hat{q}$, proportion of asymptomatic individuals ρ, recovery rate γ, and hospitalisation rate δ. Darker shading indicates a higher R_0. We see that R_0 is most sensitive to $\hat{q}$ and γ; reducing transmission or shortening the infectious duration yields the greatest decline in R_0. Figure 9 repeats these comparisons but now varies the overall contact-mixing scale λ vs. each of ρ, γ, and δ in the same six-panel layout. We deduce that interventions aimed at minimising contact, in conjunction with key measures such as improving recovery through treatment, are crucial to effectively manage the spread of the disease.

5 Discussion and Conclusion

This study presented a compartmental model that stratifies the population by 21 age bands and 10 deprivation deciles, extending the classic SEIR framework to eight compartments: susceptible, exposed, asymptomatic, undetected symptomatic, detected symptomatic, hospitalised, recovered, and dead. This layered structure allowed us to capture two critical factors: age-dependent contact patterns (using the POLYMOD

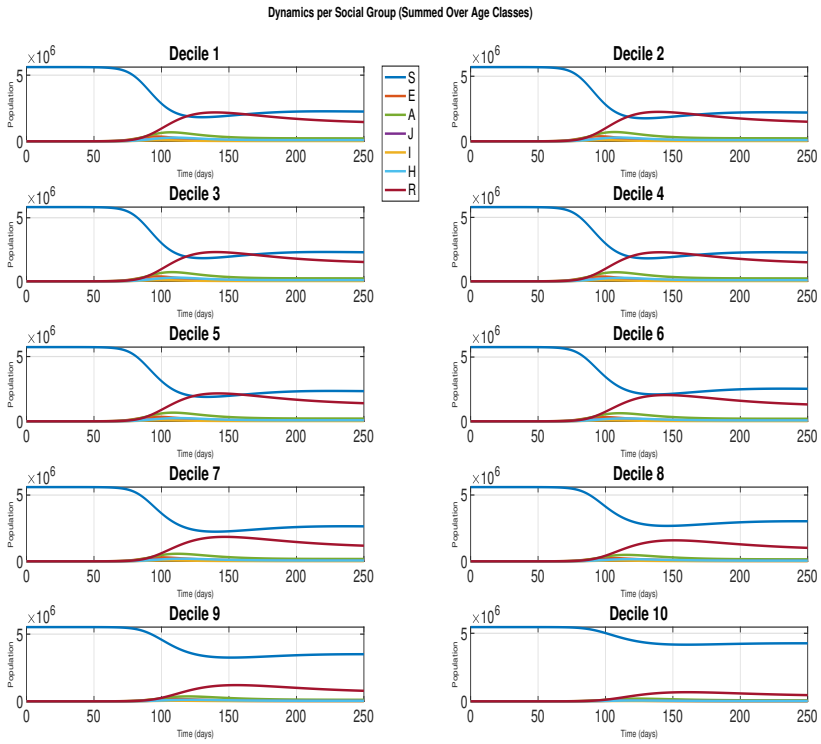

Fig 6. Time series of all epidemiological compartments aggregated over age for each deprivation decile. Panels1–10 correspond to deciles1 (most deprived) to10 (least deprived). For each, the curves show the susceptible, exposed, asymptomatic, symptomatic (detected and undetected), hospitalised, and recovered populations over 150 days. More deprived deciles peak earlier and at higher magnitudes in infectious and hospitalised cases, reflecting denser contact patterns.

matrix) and socioeconomic mixing (using a deprivation-decile interaction matrix). By combining the two factors into a single "who-acquires-infection-from-whom" block matrix $\boldsymbol{\lambda_{i,n,j,k}}$, we derived an expression for the basic reproduction number, as presented in equation (12), whose dominant eigenvalue quantifies the average number of secondary cases in a fully susceptible, stratified population. By examining the maximum eigenvalues of each block, we further decomposed the transmission contributions within and between deprivation deciles.

Analytically, we demonstrated the positivity and boundedness of all compartments, ensuring the absence of negative populations or unbounded growth. Using the next-generation matrix method, we showed that when $R_0 < 1$, the DFE is asymptotically stable both locally and globally. This guarantees eventual epidemic extinction, regardless of the initial conditions. Additionally, we show that a unique endemic equilibrium exists and is globally asymptotically stable when $R_0 > 1$. This confirms sustained transmission in the absence of interventions.

Sensitivity analysis, both analytical and numerical, revealed the parameter that most strongly drives the value of R_0. The contact rate $\boldsymbol{\lambda_{i,n,j,k}}$ has a normalised sensitivity index of 1, as shown in Figure 3. This implies that a 1% increase in the overall mixing directly translates to a 1% increase in the value of R_0. The fraction of asymptomatic

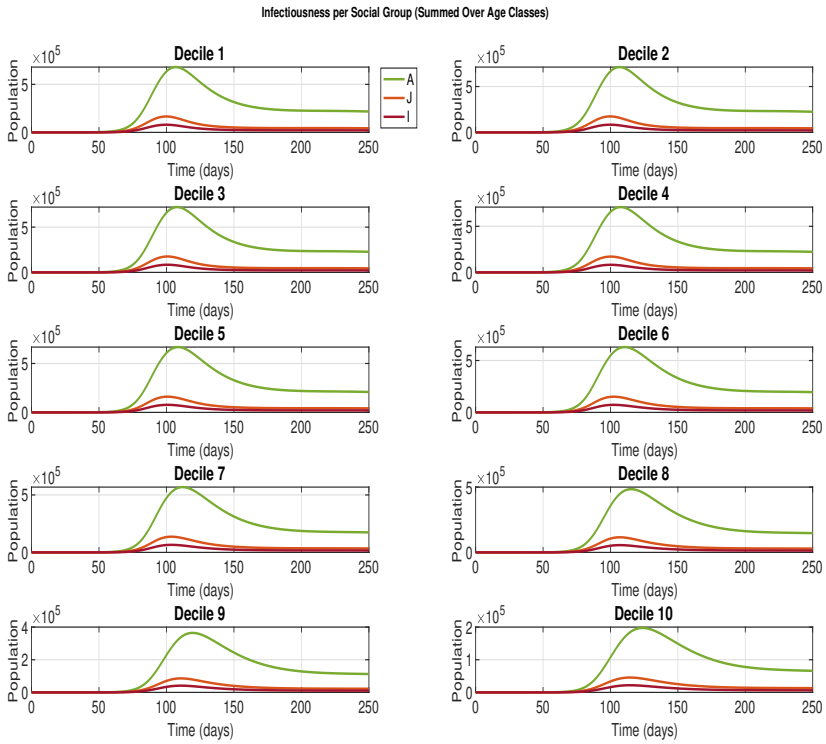

Fig 7. Infection trajectories by deprivation decile, aggregated over age groups. For each decile (1=most deprived. . . 10=least deprived), the curves show asymptomatic (green), detected symptomatic (red), and undetected symptomatic (orange), populations over 250 days. More-deprived deciles peak earlier and reach higher burdens in the infectious compartments.

individuals ρ, recovery rate γ, and hospitalisation rate δ (in the sensitivity plot Figure 3, we took the average rate across all age groups) have a significant impact on R_0, whereas the testing coverage π and modification factor ι have a minor influence on R_0. The findings suggest that keeping track of the "hidden" effects of asymptomatic transmission, shortening the infectious periods, and lowering hospitalisation rates—which, in our scenario, could serve as "treatment" since we assumed that hospitalised individuals do not further contribute to infection—are nearly as crucial as decreasing contact during an outbreak. The insignificant impact of the testing rate in Figure 3 could be attributed to the negligible value of the test proportion during the initial phase of the pandemic.

Parameter $\pi(t)$ represents the fraction of all infected individuals identified (tested) at time t. These detected individuals are assumed to isolate (or be isolated) and have reduced onwards transmission (modified by the parameter $\iota \ll 1$), whereas undetected infectious individuals (fraction $1 - \pi(t)$) continue to spread with full transmissibility. However, improving the testing capacity is critical in reduction infection transmissibility, as shown in Figure 4.Although it may not lower the reproduction number (R_0) to below one on its own, it can substantially decrease R_0. However, when paired with measures like contact reduction, strict isolation, vaccination, and so on, it could potentially bring R_0 below 1, thus curbing the epidemic's spread. This is plausible because testing individuals alone without taking necessary actions towards isolation or treatment will be

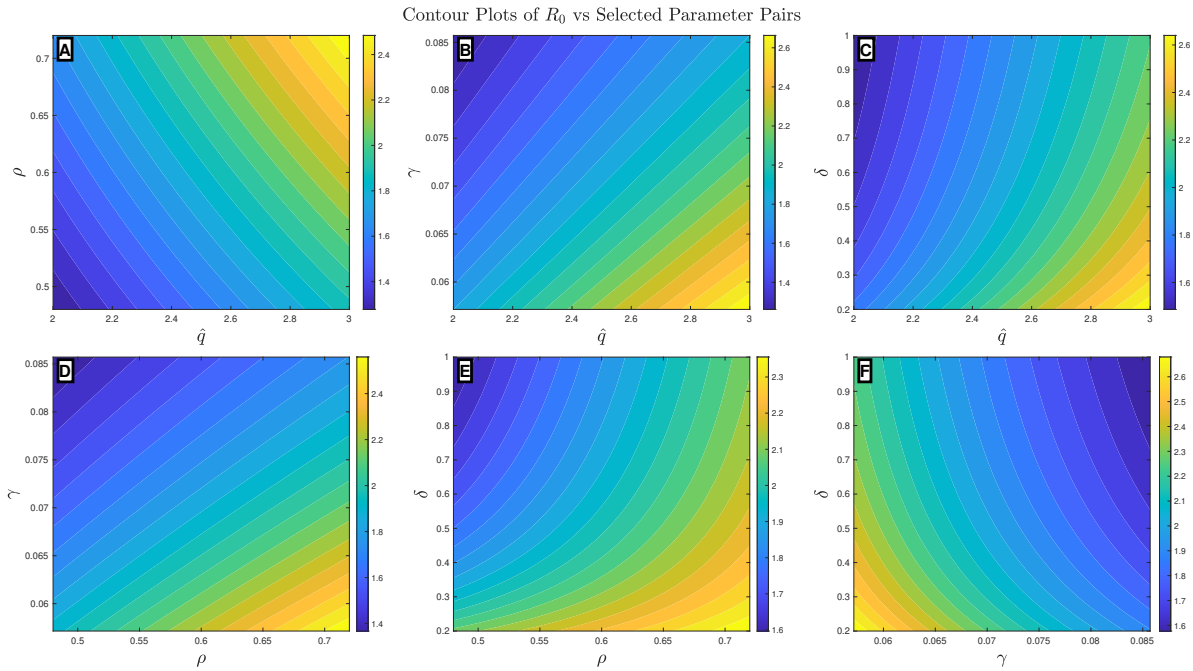

Fig 8. Contour plots illustrating the sensitivity of the basic reproduction number R_0 to pairwise variations in the key epidemiological parameters. Each panel shows R_0 computed over a $\pm 20\,\%$ grid around the baseline values of the two parameters, with all other parameters fixed. δ_i the rate of hospitalisation by age group is scaled to δ by the value $[0.2, 1]$. The pairs of parameters are (A) relative transmission rate $\hat{q}$ vs asymptomatic fraction ρ, (B) $\hat{q}$ vs recovery rate γ, (C) $\hat{q}$ vs hospitalisation rate δ, (D) ρ vs γ, (E) ρ vs δ, and (F) γ vs. δ. Shading denotes the magnitude of R_0 according to the adjacent colour bar.

counter-intuitive. *Contreras et al.* [41] confirm that solely relying on testing, tracing, and isolation is inadequate for controlling the spread of COVID-19, unless these measures are integrated with additional pharmaceutical or non-pharmaceutical strategies.

Figure 8 shows how pairwise changes in key epidemiological parameters jointly shape the basic reproduction number R_0. In Panel A, we vary the relative transmission rate $\hat{q}$ relative to the fraction of asymptomatic individuals ρ. The contours slope upward, indicating that an increase in either $\hat{q}$ or ρ drives R_0. A combination of both can significantly alter the trajectory of an epidemic. Panels B and C replace ρ with recovery rate γ and hospitalisation rate δ, respectively. If recovery and treatment is lower, and the relative transmission rate is higher, an increase transmissibility due to increased value of R_0 is observed. Panels D–F repeat these explorations for the remaining parameter pairs (ρ vs. γ, ρ vs. δ, and γ vs. δ, respectively). In Panels D and E, increasing recovery or hospitalisation can keep R_0 values low if only we can keep the number of asymptomatic individuals relatively low. This shows that when infectious individuals are removed quickly through recovery or clinical isolation, the amplifying effect of hidden (asymptomatic) transmission could be substantially blunted. Panel F illustrates that a longer duration to recovery combined with reduced hospitalization rates correlates with an increased value of R_0. This emphasizes the critical role of timely clinical care. Figure 9 repeats these comparisons but now varies the scaled overall contact-mixing (λ) vs. each of ρ, γ, and δ. We deduce that interventions aimed at minimising contact or social interactions, in conjunction with key measures such as

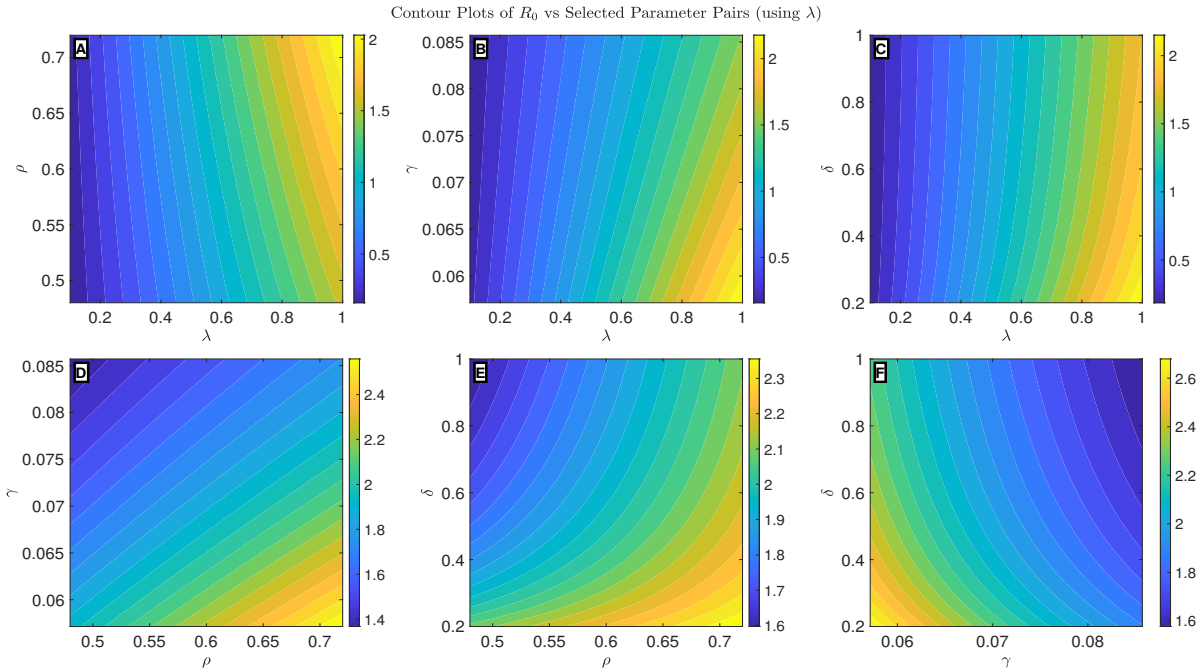

Fig 9. Contour plots illustrating the sensitivity of the basic reproduction number R_0 to pairwise variations in key epidemiological parameters. Each panel shows R_0 computed over a $\pm 20\,\%$ grid around the baseline values of the two parameters, with all other parameters fixed. The contact mixing matrix is scaled between $[0.1, 1]$ and δ_i the rate of hospitalisation by age group is scaled to δ by the value $[0.2, 1]$. The pairs of parameters are (A) scaled contact matrix λ vs asymptomatic fraction ρ, (B) λ vs recovery rate γ, (C) λ vs hospitalisation rate δ, (D) ρ vs γ, (E) ρ vs δ, and (F) γ vs δ. The shading denotes the magnitude of R_0 according to the adjacent colour bar.

improving recovery through treatment, are crucial to effectively manage the spread of the disease.

By integrating age-structured contact data with a novel deprivation-decile mixing framework, this model provides a rigorous yet practical tool for understanding and controlling infectious diseases such as COVID-19. Analytical evidence and numerical findings indicate that reducing contact mixing and relative transmission rates, along with rapid recovery and treatment, is crucial for lowering the disease burden during infection outbreaks. This aligns with findings in the literature [33, 35, 40] that significantly decreasing the contact rate combined with timely enhancement of hospital treatment can lead to more effective disease control.

Acknowledgments

We acknowledge the support of the Institute for Global and Pandemic Planning (IGPP) at the University of Warwick. MJT is supported by the Biotechnology and Biological Sciences Research Council (BBSRC) and University of Warwick funded Midlands Integrative Biosciences Training Partnership (MIBTP) [Grant Number BB/M01116X/1].

References

1. Sadeghi Dousari, A., Taati Moghadam, M. & Satarzadeh, N. Covid-19 (coronavirus disease 2019): a new coronavirus disease. *Infection and drug resistance* 2819–2828 (2020).

2. Sameni, R. Mathematical modeling of epidemic diseases; a case study of the covid-19 coronavirus, DOI: 10.48550/arxiv.2003.11371 (2020).

3. Keeling, M. J. *et al.* Fitting to the uk covid-19 outbreak, short-term forecasts and estimating the reproductive number, DOI: 10.1101/2020.08.04.20163782 (2020).

4. Keeling, M. J. *et al.* Predictions of covid-19 dynamics in the uk: Short-term forecasting and analysis of potential exit strategies. *International Society for Computational Biology* **17**, e1008619–e1008619, DOI: 10.1371/journal.pcbi.1008619 (2021).

5. Hollingsworth, T. D. Controlling infectious disease outbreaks: Lessons from mathematical modelling. *Palgrave Macmillan* **30**, 328–341, DOI: 10.1057/jphp.2009.13 (2009).

6. Feng, Z. *et al.* Timely identification of optimal control strategies for emerging infectious diseases. *Elsevier BV* **259**, 165–171, DOI: 10.1016/j.jtbi.2009.03.006 (2009).

7. Keeling, M. J. & Danon, L. Mathematical modelling of infectious diseases. *British Medical Bulletin* **92**, 33–42, DOI: 10.1093/bmb/ldp038 (2009). https://academic.oup.com/bmb/article-pdf/92/1/33/954051/ldp038.pdf.

8. Keeling, M. J. & Rohani, P. Modeling infectious diseases in humans and animals, DOI: 10.2307/j.ctvcm4gk0 (2011).

9. Bernoulli, D. & Blower, S. An attempt at a new analysis of the mortality caused by smallpox and of the advantages of inoculation to prevent it. *Wiley* **14**, 275–288, DOI: 10.1002/rmv.443 (2004).

10. Bacaër, N. Daniel bernoulli, d'alembert and the inoculation of smallpox (1760), DOI: 10.1007/978-0-85729-115-8_4 (2011).

11. Kermack, W. O. & McKendrick, A. G. Contributions to the mathematical theory of epidemics. ii. —the problem of endemicity. *Royal Society* **138**, 55–83, DOI: 10.1098/rspa.1932.0171 (1932).

12. Kermack, W. O. & McKendrick, A. G. Contributions to the mathematical theory of epidemics iv. analysis of experimental epidemics of the virus disease mouse ectromelia. *Cambridge University Press* **37**, 172–187, DOI: 10.1017/s0022172400034902 (1937).

13. Ross, R. S. The mathematics of malaria. *BMJ* **1**, 1023–1023, DOI: 10.1136/bmj.1.2626.1023 (1911).

14. Hoppensteadt, F. C. An age dependent epidemic model. *Elsevier BV* **297**, 325–333, DOI: 10.1016/0016-0032(74)90037-4 (1974).

15. Kumar, M. & Abbas, S. Age-structured sir model for the spread of infectious diseases through indirect contacts. *Mediterranean Journal of Mathematics* **19**, 14 (2022).

16. Davies, N. G. *et al.* Age-dependent effects in the transmission and control of covid-19 epidemics. *Nature medicine* **26**, 1205–1211 (2020).

17. Pellis, L., Cauchemez, S., Ferguson, N. M. & Fraser, C. Systematic selection between age and household structure for models aimed at emerging epidemic predictions. *Nature communications* **11**, 906 (2020).

18. Chhetri, B., Vamsi, D., Prakash, D. B., Balasubramanian, S. & Sanjeevi, C. B. Age structured mathematical modeling studies on covid-19 with respect to combined vaccination and medical treatment strategies. *Computational and Mathematical Biophysics* **10**, 281–303 (2022).

19. Jing, S., Xue, L., Li, X., Zeng, F. & Yang, J. Age-structured modeling of covid-19 dynamics: the role of treatment and vaccination in controlling the pandemic. *Journal of Mathematical Biology* **90**, 1–49 (2025).

20. O'Driscoll, M. *et al.* Age-specific mortality and immunity patterns of sars-cov-2. *Nature Portfolio* **590**, 140–145, DOI: 10.1038/s41586-020-2918-0 (2020).

21. Spi-m-o: Statement on population segmentation by age group (2020).

22. Hilton, J. & Keeling, M. J. Estimation of country-level basic reproductive ratios for novel coronavirus (sars-cov-2/covid-19) using synthetic contact matrices. *PLoS computational biology* **16**, e1008031 (2020).

23. House, T. & Keeling, M. J. Household structure and infectious disease transmission. *Epidemiology & Infection* **137**, 654–661 (2009).

24. Koh, D. Occupational risks for covid-19 infection (2020).

25. Hilton, J. & Keeling, M. J. Incorporating household structure and demography into models of endemic disease. *Royal Society* **16**, 20190317–20190317, DOI: 10.1098/rsif.2019.0317 (2019).

26. Manna, A., Koltai, J. & Karsai, M. Importance of social inequalities to contact patterns, vaccine uptake, and epidemic dynamics. *Nature Communications* **15**, 4137 (2024).

27. Manna, A., Dall'Amico, L., Tizzoni, M., Karsai, M. & Perra, N. Generalized contact matrices allow integrating socioeconomic variables into epidemic models. *Science Advances* **10**, eadk4606 (2024).

28. Munday, J. D., van Hoek, A. J., Edmunds, W. J. & Atkins, K. E. Quantifying the impact of social groups and vaccination on inequalities in infectious diseases using a mathematical model. *BioMed Central* **16**, DOI: 10.1186/s12916-018-1152-1 (2018).

29. Hale, A. C., Read, J. M. & Jewell, C. Modelling the impact of social mixing and behaviour on infectious disease transmission: application to sars-cov-2, DOI: 10.48550/arxiv.2211.02371 (2022).

30. Munday, J. D., van Hoek, A. J., Edmunds, W. J. & Atkins, K. E. Quantifying the impact of social groups and vaccination on inequalities in infectious diseases using a mathematical model. *BMC medicine* **16**, 1–12 (2018).

31. Mossong, J. *et al.* Social contacts and mixing patterns relevant to the spread of infectious diseases. *PLoS medicine* **5**, e74 (2008).

32. Hethcote, H. W. Modeling heterogeneous mixing in infectious disease dynamics. *Models for infectious human diseases: their structure and relation to data* **215**, 238 (1996).

33. Keeling, M. J. *et al.* Precautionary breaks: Planned, limited duration circuit breaks to control the prevalence of sars-cov2 and the burden of covid-19 disease. *Epidemics* **37**, 100526 (2021).

34. Muller, K. & Muller, P. A. Mathematical modelling of the spread of covid-19 on a university campus. *Infectious Disease Modelling* **6**, 1025–1045 (2021).

35. Anggriani, N. & Beay, L. K. Modeling of covid-19 spread with self-isolation at home and hospitalized classes. *Results in Physics* **36**, 105378 (2022).

36. Hale, A. C., Read, J. M. & Jewell, C. P. Modelling the impact of social mixing and behaviour on infectious disease transmission: application to sars-cov-2. *arXiv preprint arXiv:2211.02371* (2022).

37. Wu, K., Darcet, D., Wang, Q. & Sornette, D. Generalized logistic growth modeling of the covid-19 outbreak: comparing the dynamics in the 29 provinces in china and in the rest of the world. *Nonlinear dynamics* **101**, 1561–1581 (2020).

38. Wodajo, F. A., Gebru, D. M. & Alemneh, H. T. Mathematical model analysis of effective intervention strategies on transmission dynamics of hepatitis b virus. *Scientific Reports* **13**, 8737 (2023).

39. Al-arydah, M. Assessing vaccine efficacy for infectious diseases with variable immunity using a mathematical model. *Scientific Reports* **14**, 18572 (2024).

40. Zhang, J. *et al.* Changes in contact patterns shape the dynamics of the covid-19 outbreak in china. *Science* **368**, 1481–1486 (2020).

41. S. Contreras, J. Dehning, M. Loidolt, J. Zierenberg, F. P. Spitzner, J. H. Urrea-Quintero, S. B. Mohr, M. Wilczek, M. Wibral, and V. Priesemann, "The challenges of containing SARS-CoV-2 via test-trace-and-isolate," *Nature Communications*, vol. 12, no. 1, p. 378, 2021.